Gravity flow in rock fractures with substrate and edge drainage

[1]N. Merli, [1]S. Longo, [1]L. Chiapponi [2]V. Di Federico

[1]*Dipartimento di Ingegneria e Architettura - Università degli Studi di Parma -*
Parco Area delle Scienze 181/A - 43124 Parma - Italy

[2]*Dipartimento di Ingegneria Civile, Chimica, Ambientale e dei Materiali (DICAM),*
Università di Bologna, Viale Risorgimento, 2, 40136 Bologna,
Italy[a]

We investigate the influence of fluid rheology on flow in a finite rock fracture with vertically varying aperture and subject to competing drainage mechanisms due to a permeable substrate and a draining edge. The flow is due to the release of a finite volume of fluid and the rheology of the fluid is either Newtonian, Ostwald-deWaele, or Herschel-Bulkley. The Hele-Shaw analogy between lubrication and seepage flows allows extending our results to a porous medium with permeability and porosity varying in the vertical direction. The general solution is numerical, except for a self-similar solution derived for Newtonian fluids in a constant aperture fracture and another for Ostwald-deWaele fluids without substrate drainage. Results for the profile of the current and the volume remaining within the fracture, and drained at the substrate and edge, depend on a dimensionless parameter λ incorporating fluid rheology, fracture geometry, and ambient depth; drainage times exhibit order of magnitude variations depending on λ. A second dimensionless parameter, λ', intervenes for Herschel-Bulkley fluids, with $\lambda' \to \infty$ for Ostwald-deWaele fluids. The theoretical model is validated with a series of experiments conducted with a novel experimental apparatus, accurately reproducing the condition of substrate drainage and allowing the experimental determination of λ and λ'. The agreement between theory and experimental results for both configurations with constant and V-shaped aperture is quite good, considering model approximations and experimental uncertainties. The present analysis shows how domain anisotropy, though simply schematized, and fluid rheology are relevant for the correct estimation of all integral variables, such as the residual fluid volume in the fracture as a function of time.

Keywords: gravity currents, non-Newtonian, rock fracture, variable aperture, drainage, experiments.

---

[a] Email address for correspondence: luca.chiapponi@unipr.it

I.   INTRODUCTION

A broad category of gravity-driven flows, whether in porous media and fractures or in other environments, occur in the presence of two fluids of different densities, one intruding into the other. The categories of environmental flows that can be classified as gravity-driven flows are numerous and manifold, as reflected in the literature cited and commented on in Simpson[1], Huppert[2], Ungarish[3]; these include, but are not limited to, CO_2 sequestration or environmental remediation. For this reason, the search for conceptual models, corroborated by experiments, has been particularly fruitful.

Gravity currents in porous and fractured media have been extensively studied, considering impermeable or permeable boundaries[4–9], and anisotropy in the horizontal or vertical direction[10,11]. Other than the drainage effect due to the substrate[12,13], edge drainage effects associated with the finiteness of the domain significantly influence the shape of the gravity current, with implications for the specific problem at hand, as shown by Zheng *et al.*[14] for both a homogeneous porous medium and a porous medium with a vertical increase in permeability and porosity. When both drainage mechanism are present, they compete[15].

The influence of the fluid rheology, typically considered to be Newtonian in earlier formulations, was analysed considering both Ostwald-deWaele (OdW)[11,16,17] and Herschel-Bulkley (HB) fluids[18]; in some works, non-Newtonian behaviour was coupled with anisotropy[19]. Among all contributions, several include an experimental validation in addition to the theoretical model, of an analytical (often self-similar) and numerical nature.

In passing, we recall that the well-known Hele-Shaw (HS) analogy between fracture and porous media flow was extended to OdW fluids in various geometries[20,21].

A review of the possible implications of drainage, confinement, anisotropy, and flow convergence in porous media can be found in Zheng & Stone[22].

In the present work, we consider a specific domain geometry, a vertical fracture limited below by a crack of lower permeability, and laterally by a single draining edge. Such a geometry has already been studied by Yu *et al.*[15] deriving a theoretical model for Newtonian flow under conditions of constant volume or flow injection.

In a more generalized view, the phenomenon under investigation is framed in the studies for CO_2 sequestration; these also consider the process of leakage resulting from fractures, pre-existing or intervening, in the cap rock bordering the aquifer. In essence, the proposed

geometry refers to a plume of CO_2 under supercritical conditions (i) injected in the aquifer, and (ii) propagating away from the injection well moving in contact with the cap rock, also (iii) percolating through a lower permeability layer, (iv) and reaching a vertical fracture of such permeability characteristics that it completely drains the fluid without allowing further advancement of the front. To predict the short and long term fate of the fluid in this configuration, it is essential to predict the behaviour of the current in the presence of leaky boundaries.

This coupled drainage could also occur, for example, when a front initially advancing over a permeable substrate reaches the vertical fracture; in such a case there is a competitive mechanism whereby if the drainage at the bottom compensates for the incoming flow, the current fails to reach the vertical fracture, which represents localized drainage, and the problem is a moving boundary one, since the position of the current front is not known a priori; or the front reaches the fracture and the problem is transformed into a fixed geometry problem, with the length of the current geometrically known. A second important distinction is between the release of a constant volume of fluid, and the injection of fluid with constant or time-varying flow rate. In addition, it is possible to consider non-homogeneity and anisotropy, coherently with the inherent heterogeneity and anisotropy of fractured rocks at all scales[23,24].

Also for CO_2 studies, it is of interest to consider a non-Newtonian rheology of the fluid, which adds a level of complexity and which in many cases renders the model more adherent to physical reality: for example, surfactant based CO_2 foams used in industrial applications[25], as well as liquid adsorbents used for CO_2 capture[26], exhibit non-Newtonian shear-thinning behaviour. The simplest model of shear-thinning behaviour is the Ostwald-DeWaele (OdW), or power-law model, including two parameters; if yield stress is present, the Herschel-Bulkley model (HB), having three parameters, is typically adopted.

Thus the present analysis refers to a gravity current of a OdW or HB fluid advancing in a fracture with aperture, and hence permeability, increasing in the vertical direction while remaining uniform in the horizontal direction. The Newtonian fluid and the uniform aperture are special cases. Drainage occurs at the bottom and at one end of the domain. We specifically analyse the constant volume condition that is progressively depleted by drainage. Noteworthy, our results are novel also for a Newtonian fluid, as free-surface flow in a variable aperture fracture of finite length was never studied in conjunction with both
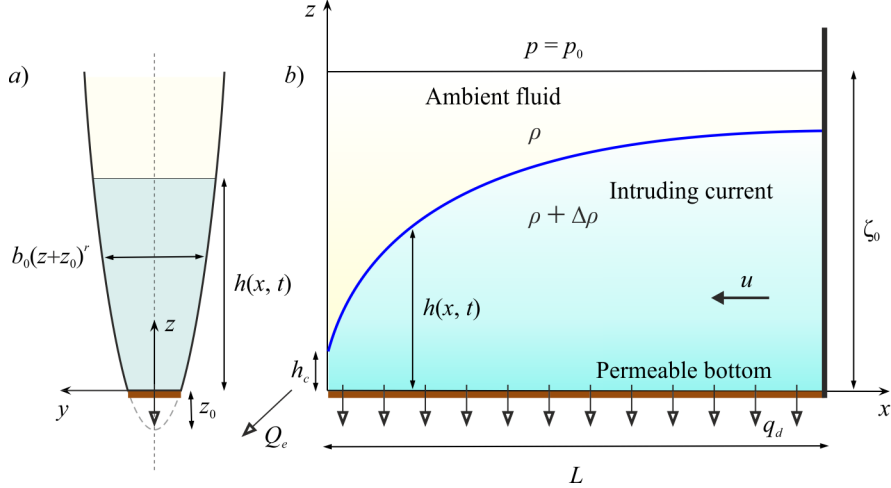
FIG. 1. Schematics of the problem with fluid drainage from a permeable bottom and a fixed edge. a) Cross-section, and b) side view. The figure is not to scale as $h(x,t) \ll \zeta_0$.

edge and substrate drainage.

The paper is organized as follows. Section II illustrates the theoretical model for both rheologies adopted, section III describes the experimental layout and procedures, section III A provides details and discussion on the experiments. Conclusions are drawn in section IV. Appendix A provides details about the calibration procedure leading to the determination of a dimensionless parameter quantifying the intensity of substrate drainage, and Appendix B includes further details about the experiments.

II. THEORETICAL MODEL

A. Formulation for OdW fluid flowing in a fracture with vertically varying aperture

Consider the transient motion of a gravity current in a vertical fracture, or HS cell, initially saturated with an ambient fluid of height ζ_0 subject to both edge and substrate drainage[15], see figure 1; the substrate drainage is due to a draining, underlying crack with the same length L and an aperture b_b much narrower than that b_0 of the main fracture (see figure 2), i.e. $b_b \ll b_0$; the bottom crack is entirely saturated. The substrate drainage is a gravity-driven vertical flow rate per unit length, i.e. dependent on the local height of the overlying current; as the thickness of the substrate is much smaller than the gravity

5

current height (the 'shallow crack' assumption, see[27]), the flow in the permeable substrate is not modelled in detail, as it would be with the 'deep crack' assumption[13,28]. While a shallow, draining crack is adopted in the model and experiments, it should be noted that it is equivalent to a thin porous medium (see for this case Pritchard *et al.*[28]) as the Hele-Shaw analogy is well-established for both Newtonian and non-Newtonian power-law fluids, see for the latter case the works of Longo *et al.*[9] and Ciriello *et al.*[20].

The edge drainage modifies the profile of the current thereby affecting the substrate drainage; thus the evolution of the gravity current is modulated by these two outflows. The motion induced by the advancement of the intruding current in the ambient is neglected, which is tantamount to say that the current height $h(x,t) \ll \zeta_0$. We consider a finite-volume release problem, with a given volume of fluid initially at rest.

We further assume that the fracture, of finite length L, has an aperture symmetric with respect to the z axis and increasing along the vertical direction according to the power function $b = b_0(z + z_0)^r$ (Figure 1), where $b_0 z_0^r$ is the width of the gap at the permeable substrate and $0 \le r \le 1$ controls the fracture rate of widening along the vertical; for $r = 0$, $b(z) = b_0$; for $r = 1$, the fracture is triangular; these are the two most relevant cases. The aperture is invariant in the longitudinal direction x; further model refinements may include variations along the direction of propagation.

The rheology of the current is modelled according to the OdW model, with $\tau = \mu_0 |\dot{\gamma}|^{n-1}\dot{\gamma}$, where τ is the shear stress, μ_0 is the fluid consistency, and n is the fluid behaviour index, with $n < 1$ representing shear-thinning and $n > 1$ shear-thickening behaviour, respectively, and $n = 1$ the Newtonian one; in the latter case, μ_0 becomes the dynamic viscosity. The OdW model can be expressed in tensorial form for a generic three-dimensional flow, but we limit our analysis to one-dimensional flows. In the geometry shown in figure 1, the model reads

$$\tau_{yx} = \mu_0 \left| \frac{\partial u}{\partial y} \right|^{n-1} \frac{\partial u}{\partial y}, \tag{1}$$

where y is the cross-aperture direction and τ_{yx} is the shear stress acting on surfaces normal to y in the $x-$direction.

The fluid has a density $\rho + \Delta\rho$, where ρ is the ambient fluid density. We assume that the interface between the ambient and the propagating current is sharp (without diffusion), and that the ratio between the thickness of the current and its length is small. We also neglect surface tension. In these conditions, a hydrostatic pressure distribution holds, with

$p(x, z, t) = p_0 + \Delta \rho g[h(x, t) - z] + \rho g(\zeta_0 - z)$, where $p_0 = p(\zeta_0)$.

To derive the momentum balance equation for the geometry of Figure 1, we note that inertial effects can be neglected for low Reynolds number flow, thus the balance is between the relevant normal stress and the tangential stresses, leading to

$$\frac{\partial \tau_{zx}}{\partial z} + \frac{\partial \tau_{yx}}{\partial y} + \frac{\partial p}{\partial x} = 0. \tag{2}$$

At any height z along the fracture, it is verified that $b(z) \ll L$; this justifies the one-dimensional approximation implicit in eq. (1) as $\tau_{zx} \ll \tau_{yx}$; furthermore, it entails that the gravity current depth h has a negligible variation along the transversal direction y, i.e. $\partial h / \partial y = 0$.

Hence, eq. (2) reduces to

$$\frac{\partial \tau_{yx}}{\partial y} + \frac{\partial p}{\partial x} = 0, \tag{3}$$

with a driving pressure gradient equal to

$$\frac{\partial p}{\partial x} = \Delta \rho \, g \frac{\partial h}{\partial x}; \tag{4}$$

Inserting eq. (1) in eq. (3) yields upon integration with the no slip condition at the walls $y = \pm (b_0/2)(z + z_0)^r$ and the null shear stress condition at $y = 0$

$$u(x, y, z, t) = -\frac{n}{n+1} \left[\left(\frac{b_0(z + z_0)^r}{2} \right)^{1+1/n} - |y|^{1+1/n} \right] \frac{\partial h}{\partial x} \left| \frac{\partial h}{\partial x} \right|^{1/n-1} \left(\frac{\Delta \rho \, g}{\mu_0} \right)^{1/n}. \tag{5}$$

The aperture-averaged fluid velocity is

$$u(x, z, t) = -\frac{n}{2n+1} \left[\frac{b_0}{2} (z + z_0)^r \right]^{1+1/n} \left| \frac{\partial h}{\partial x} \right|^{1/n-1} \frac{\partial h}{\partial x} \left(\frac{\Delta \rho \, g}{\mu_0} \right)^{1/n}, \tag{6}$$

and the spatially variable flow rate takes the form

$$Q(x, t) = \int_0^h u(x, z, t) b_0 (z + z_0)^r \mathrm{d}z = -\frac{n^2}{(2n+1)[r(2n+1)+n]} b_0 \left(\frac{b_0}{2} \right)^{1+1/n} \left| \frac{\partial h}{\partial x} \right|^{1/n-1} \times$$
$$\frac{\partial h}{\partial x} \left(\frac{\Delta \rho \, g}{\mu_0} \right)^{1/n} \left[(h(x, t) + z_0)^{r(2+1/n)+1} - z_0^{r(2+1/n)+1} \right], \tag{7}$$

with a cross-sectional area equal to

$$A(x, t) = \frac{b_0}{r+1} \left[(h(x, t) + z_0)^{r+1} - z_0^{r+1} \right]. \tag{8}$$
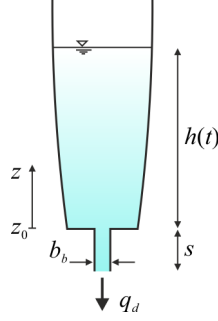
FIG. 2. A narrow fracture (crack) of aperture b_b draining the main upper fracture.

Under the previous assumptions, the local continuity equation reads

$$\frac{\partial Q}{\partial x} + \frac{\partial A}{\partial t} + q_d = 0, \tag{9}$$

where Q is the volumetric flow rate in the fracture, A is the cross-sectional area of the gravity current and q_d is the drained flow rate per unit length.

The latter quantity is evaluated as follows for a draining crack (the porous medium version is easily developed with minor modifications). We start from eq. (6), insert the width of the draining fracture b_b in lieu of the width b of the HS cell, and assume that the pressure gradient is proportional to $(h(x,t) - z_1)/s$, obtaining

$$q_d(x,t) = b_b \frac{n}{2n+1} \left(\frac{b_b}{2}\right)^{1+1/n} \left(\frac{\Delta \rho\, g}{\mu_0}\right)^{1/n} \left(\frac{h(x,t) - z_1}{s}\right)^{1/n}, \tag{10}$$

where s is the length of the draining fracture in the vertical direction, and z_1 is the fluid level, or head, at its outflow in the longitudinal direction. Inserting eqs. (7–10) in eq. (9) yields

$$\frac{b_0}{r+1} \frac{\partial}{\partial t} \left[(h+z_0)^{r+1}\right] - \frac{n^2}{(2n+1)[r(2n+1)+n]} b_0 \left(\frac{b_0}{2}\right)^{1+1/n} \left(\frac{\Delta \rho\, g}{\mu_0}\right)^{1/n}$$
$$\times \frac{\partial}{\partial x} \left[\left|\frac{\partial h}{\partial x}\right|^{1/n-1} \frac{\partial h}{\partial x} \left((h+z_0)^{r(2+1/n)+1} - z_0^{r(2+1/n)+1}\right)\right] +$$
$$b_b \frac{n}{2n+1} \left(\frac{b_b}{2}\right)^{1+1/n} \left(\frac{\Delta \rho\, g}{\mu_0}\right)^{1/n} \left(\frac{h - z_1}{s}\right)^{1/n}. \tag{11}$$

Initial and boundary conditions are as follows. We consider a rectangular profile that initially fills the domain, so the initial condition is of uniform height of the current, $h(x,0) = h_0$, while the upstream boundary condition at $x = L$ is of zero influx, equivalent to $\partial h/\partial x(L,t) =$

8

0. We then assume a free fall in the origin $x = 0$, with a current depth equal to the critical height h_c. The latter concept, widely adopted in the one-dimensional theory of open-channel flow (see, e.g., the classical book by Chow[29]) stems from the fact that the variation of specific energy (energy per unit weight) at a constant discharge shows a minimum at a depth called critical height, at which the Froude number is unity. The expression implicitly defining h_c is then

$$\frac{\partial}{\partial h}\left[h + \alpha \frac{V^2}{2g}\right] \equiv \frac{\partial}{\partial h}\left[h + \alpha \frac{Q^2}{2gA^2}\right] = 0, \tag{12}$$

where the mass balance equation $Q = VA$ was employed, h, $Q(h)$, $V(h)$, $A(h)$ are the height, discharge, average velocity, and cross-sectional area of the current, and $\alpha \geq 1$ is the Coriolis velocity-head coefficient, or kinetic power coefficient, defined as

$$\alpha(x, t) = \frac{A^2 \int_A u(x, y, z, t)^3 \, dA}{\left(\int_A u(x, y, z, t) \, dA\right)^3}. \tag{13}$$

The Coriolis coefficient given by (13) stems from the fact that the velocity head for a current is greater than the value computed from the expression $V^2/2g$, as the square of the average velocity is less than the weighted average of the squares of local velocities.

Next, eq. (12) can be written as

$$1 - \alpha_c \frac{Q^2}{gA_c^3} \frac{\partial A}{\partial h}\bigg|_c = 0 \rightarrow 1 - \alpha_c \frac{Q^2(r+1)^3}{gb_0^2(h_c + z_0)^{2r+3}} = 0. \tag{14}$$

where the subscript c indicates that the variable is computed referring to the critical height, and $\alpha = \alpha(r, n, h, z_0)$; solving eq. (14) yields h_c. The boundary condition $h(0, t) = h_c$ at the origin represents a refinement with respect to that $h(0, t) = 0$ adopted in Yu et al.[15].

1. Dimensionless form

Assuming the length scales L and h_0 (the initial current height defined above) for the horizontal and vertical directions, respectively, and a time scale $t^* = h_0/u^*$, eq. (11) becomes

$$\frac{b_0}{r+1}h_0^r u^* \frac{\partial}{\partial T}\left[(H+Z_0)^{r+1}\right] - \frac{n^2}{(2n+1)[r(2n+1)+n]}b_0\left(\frac{b_0}{2}\right)^{1+1/n}\left(\frac{\Delta\rho\, g}{\mu_0}\right)^{1/n}$$

$$\times \frac{h_0^{1/n+r(2+1/n)+1}}{L^{1+1/n}}\frac{\partial}{\partial x}\left[\left|\frac{\partial h}{\partial x}\right|^{1/n-1}\frac{\partial h}{\partial x}\left((h+z_0)^{r(2+1/n)+1}-z_0^{r(2+1/n)+1}\right)\right]+$$

$$b_b\frac{n}{2n+1}\left(\frac{b_b}{2}\right)^{1+1/n}\left(\frac{\Delta\rho\, g}{\mu_0}\right)^{1/n}\frac{h_0^{1/n}}{s^{1/n}}(H-Z_1)^{1/n}, \quad (15)$$

where the upper case denotes dimensionless counterparts of the lower case dimensional quantities. Equating the coefficients of the first two terms in eq. (15), yields

$$\frac{b_0}{r+1}h_0^r u^* = \frac{n^2}{(2n+1)[r(2n+1)+n]}b_0\left(\frac{b_0}{2}\right)^{1+1/n}\left(\frac{\Delta\rho\, g}{\mu_0}\right)^{1/n}\frac{h_0^{1/n+r(2+1/n)+1}}{L^{1+1/n}}, \quad (16)$$

resulting in the following velocity scale

$$u^* = \frac{n^2(r+1)}{(2n+1)[r(2n+1)+n]}\left(\frac{\Delta\rho\, g}{\mu_0}\right)^{1/n}\left(\frac{b_0 h_0^r}{2L}\right)^{1+1/n}h_0^{1+1/n}. \quad (17)$$

Balancing the coefficients of the first and of the last term in eq. (15) yields the parameter

$$\lambda = \frac{r(2n+1)+n}{n}\left(\frac{b_b}{b_0 h_0^r}\right)^{2+1/n}\left(\frac{L}{h_0}\right)^{1+1/n}\left(\frac{h_0}{s}\right)^{1/n} \propto \left(\frac{b_b}{b_0 h_0^r}\right)^{2+1/n}\left(\frac{L}{h_0}\right)\left(\frac{L}{s}\right)^{1/n} \quad (18)$$

which controls the flow rate drained at the substrate; the larger is λ, the larger is the substrate drainage compared to the flow through the fracture.

Equation (11) can be written in dimensionless form as

$$\frac{\partial}{\partial T}\left[(H+Z_0)^{r+1}\right] - \frac{\partial}{\partial X}\left[(H+Z_0)^{r(2+1/n)+1}\left|\frac{\partial H}{\partial X}\right|^{1/n-1}\frac{\partial H}{\partial X}\right]+$$

$$Z_0^{r(2+1/n)+1}\frac{\partial}{\partial X}\left[\left|\frac{\partial H}{\partial X}\right|^{1/n-1}\frac{\partial H}{\partial X}\right] + \lambda(H-Z_1)^{1/n} = 0. \quad (19)$$

For $r=0$, $n=1$ and $Z_0=Z_1=0$, eq. (19) reduces to

$$\frac{\partial H}{\partial T} - \frac{\partial}{\partial X}\left(H\frac{\partial H}{\partial X}\right) + \lambda H = 0, \quad (20)$$

which is identical to eq. (8a) in Yu et $al.$[15] except that λ takes a different expression here as the upper medium is fractured rather than porous and the substrate drainage is associated to a crack rather than a thin porous medium.

The boundary and initial conditions become, in dimensionless form,

$$\frac{\partial H}{\partial X}(1,T) = 0, \, H(0,T) = H_c, \, H(X,0) = 1, \, X \in [0,1], \tag{21}$$

where $H_c = h_c/h_0$.

Assuming $H(0,T) = 0$ rather than $H(0,T) = H_c$, as typically $h_c \ll h_0$ and therefore $H_c \ll 1$, the differential problem admits early-time and late-time similarity solutions for $n = 1$ (Newtonian fluid) and $r = 0$ (uniform aperture)[15]. For most other conditions, a numerical integration is required.

2. *Drainage at the vertical edge only for a OdW fluid*

Here we examine the case where the substrate drainage is zero, hence $\lambda = 0$; we also assume $Z_0 = 0$ for simplicity. Eq. (19) then becomes

$$\frac{\partial H^{r+1}}{\partial T} - \frac{\partial}{\partial X}\left(H^{r(2+1/n)+1}\left|\frac{\partial H}{\partial X}\right|^{1/n-1}\frac{\partial H}{\partial X}\right) = 0. \tag{22}$$

Looking for a self-similar solution (an intermediate asymptotic), we impose the following boundary conditions:

$$\frac{\partial H}{\partial X}(1,T) = 0, \quad H(0,T) = 0, \tag{23}$$

where, in the spirit of asymptotic self-similar solutions, the initial condition has been removed. The boundary condition at the draining edge is also simplified to $H(0,T) = 0$ (without the need of the assumption $H_c \ll 1$), based on the hypothesis that at late times, when the current has forgotten the initial condition, the profile evolves to a zero height at the edge.

The solution of eq. (22) can be expressed as $f(X,T,H) = 0$ and, for progress, we look at a group of transformations for which the differential problem described by eq. (22) with the b.c. (23) is invariant[30]. If we assume that the structure of the group is $H = \chi H', T = \beta T', X = \delta X'$, substituting into eq. (22) and imposing invariance, yields

$$\frac{\chi^{r+1}}{\beta} = \frac{\chi^{r(2+1/n)+1+1/n}}{\delta^{1+1/n}}. \tag{24}$$

Given that the problem has a geometry with a fixed longitudinal length scale L, with $0 < X < 1$, it is convenient that the variable X is invariant in the transformation, i.e. that

11

$\delta = 1$, reducing the transformation to a single parameter one. It follows that

$$\chi^{r(1+1/n)+1/n} = \beta^{-1} \to H = \beta^{-n/[r(n+1)+1]}H', \quad T = \beta T',$$ (25)

which suggests that the invariant group formed by H and T is

$$HT^{F_1}, \quad F_1 = \frac{n}{r(n+1)+1}.$$ (26)

Hence, the solution can be written as

$$f(HT^{F_1}, X) = 0 \to H \sim T^{-F_1}f(X).$$ (27)

Eq. (27) is a generalization of eqs. (2.3) and (2.10) in Zheng *et al.*[14], who studied New-tonian flow in a fracture with uniform or linearly variable aperture along the vertical. Sub-stituting eq. (27) into eq. (22) yields

$$f^{r+1} + \left(f^{r+1/F_1}f'\,|f'|^{1/n-1}\right)' = 0, f'(1) = 0, \ f(0) = 0,$$ (28)

and the dimensionless height of the current is $H = [(r+1)F_1]^{F_1})T^{-F_1}f(X)$. For $r = 0$ and $n = 1$, eq. (28) is equal to eq. (2.4*a,b,c*) in Zheng *et al.*[14]. Similarly, for $r = 1$ and $n = 1$ it equals eqs. (2.11*a,b,c*) in Zheng *et al.*[14], after rescaling the self-similar variable. Note that in many lock release problems, it is convenient for comparison purposes to express variables by introducing a time shift, see Ungarish[3]; therefore, $H = K(T+C)^{-F_1}f(X)$, with C and K positive constants.

Eq. (28) is a boundary value problem that can be integrated numerically with the shooting technique. Figure 3 shows the function $f(X)$ evaluated for varying n and r; it is seen that f decreases, from the upstream fracture end at $X = 1$ to the downstream end at $X = 0$, and is an increasing function of r, while the dependency on n, direct or inverse, is a function of fracture shape, encapsulated in r. The influence of fluid rheology on $f(X)$ turns out to be stronger for constant than for widening aperture.

The time dependence of the residual volume of fluid V_{res} in the fracture can be inferred without solving the differential problem, as

$$V_{res} = \int_0^1 H^{r+1}\mathrm{d}X = \frac{[(r+1)F_1]^{(r+1)F_1}}{T^{(r+1)F_1}}\int_0^1 f^{r+1}\mathrm{d}X,$$ (29)

or

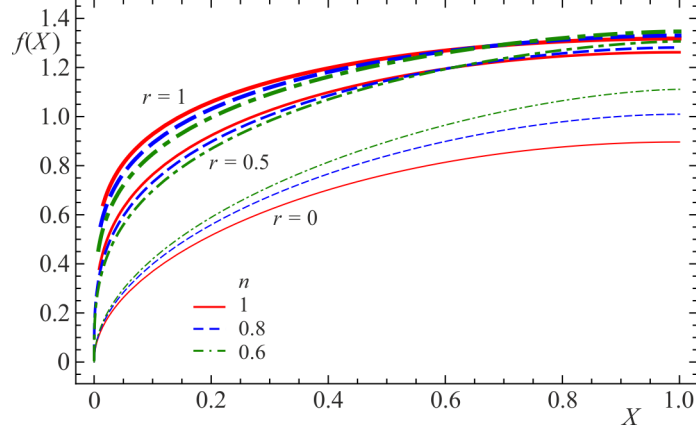$$V_{res} = \frac{[(r+1)F_1]^{(r+1)F_1}}{T^{(r+1)F_1}}\int_0^1 f^{r+1}\mathrm{d}X,$$ (30)

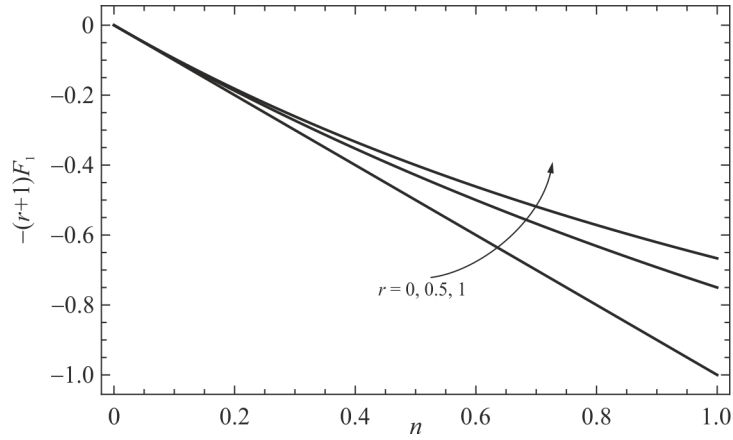FIG. 3. Self-similar solution $f(X)$ for $n = 1, 0.8, 0.6$ and for $r = 0, 0.5, 1$. Drainage is edge only.

FIG. 4. Exponent of the residual volume of fluid in the fracture versus fluid behaviour index for uniform $(r = 0)$ and upwards increasing aperture $(r = 0.5, 1)$. Drainage is edge only.

hence $V_{res} \sim T^{-(r+1)F_1}$.

Figure 4 shows the value of this time exponent as a function of fluid behaviour index n for constant $(r = 0)$ and vertically widening aperture $(r > 0)$. Emptying is faster for Newtonian than for shear-thinning fluids, and for constant than for widening aperture.

3. Drainage at the substrate only for a OdW fluid: the flow during calibration

The parameter λ could be estimated theoretically on the basis of geometrical and fluid properties. However, it is more accurate to estimate it experimentally under a well-defined flow condition. For its estimation, we proceeded to preliminary tests in which filtration

13

occurs only at the substrate, starting from a uniform initial level in the fracture. In Appendix A, we consider purely vertical flow from the main fracture into the underlying crack; applying the continuity equation to the flow of a OdW fluid in a constant aperture fracture with $r = 0$, we arrive at eq. (A4) written in dimensional form. By the inverse function rule, eq. (A4) easily transforms into:

$$\frac{\mathrm{d}t}{\mathrm{d}h} = -\frac{\left[h + \left(\frac{b_0}{b_b}\right)^n \left(\frac{K_0}{K_b}\right) s\right]^{1/n}}{h^{1/n} K_0^{-1/n} \left(\frac{\Delta \rho\, g}{\mu_0}\right)^{1/n}}, \tag{31}$$

where $K_0 = (b_0/2)^{n+1}[n/(2n+1)]^n$ and $K_b = (b_b/2)^{n+1}[n/(2n+1)]^n$ are the intrinsic permeabilities of the main fracture and of the draining crack, respectively.

Integrating eq. (31) with the initial condition $h(0) = h_0$ gives

$$t = t_0 + \left(\frac{\mu_0}{\Delta \rho\, g}\right)^{1/n} \frac{n h^{1-1/n}}{K_0^{-1/n}(1-n)} c_1^{1/n} \; {}_2F_1\left(-\frac{1}{n}, \frac{n-1}{n}; 2 - \frac{1}{n}; -\frac{h}{c_1}\right)\Bigg|_{h_0}^{h}, \tag{32}$$

where the symbol $(...)|_{h_0}^{h}$ stands for $(...)|_h - (...)|_{h_0}$, the coefficient c_1 is

$$c_1 = \left(\frac{b_0}{b_b}\right)^n \left(\frac{K_0}{K_b}\right) s, \tag{33}$$

and ${}_2F_1$ is the hypergeometric function. The parameter λ is then computed as

$$\lambda = \left(\frac{h_0}{c_1}\right)^{1/n} \left(\frac{L}{h_0}\right)^{1+1/n}. \tag{34}$$

Equation (32) is a one-parameter model to be used for estimating the value of c_1 upon comparison with the experimental height of the current over time, $h(t)$. A similar, more complex expression (not shown) was computed for λ considering a fracture with vertically varying aperture; such an expression was used for determining λ in the experiments with $r \neq 0$.

B. Coupled drainage of a Herschel-Bulkley fluid in a constant aperture fracture

The formulation outlined in §II A for a power-law fluid was extended to a HB fluid in a constant aperture fracture ($r = 0$). The HB model for a shear-thinning/thickening fluid

with yield strength τ_p is

$$\tau_{yx} = \left(\mu_0 \left| \frac{\partial u}{\partial y} \right|^{n-1} + \tau_p \left| \frac{\partial u}{\partial y} \right|^{-1} \right) \frac{\partial u}{\partial y}, \quad \tau_{yx} \geqslant \tau_p, \right\}$$
$$\left. \frac{\partial u}{\partial y} = 0, \quad \tau_{yx} < \tau_p. \right\} \tag{35}$$

With the same approach and assumptions adopted above for an OdW fluid in the case of a widening fracture, the following current profile evolution equation is obtained for an HB fluid:

$$\frac{\partial H}{\partial T} - \frac{\partial}{\partial X} \left[(H + Z_0) \left| \frac{\partial H}{\partial X} \right|^{1/n-1} \frac{\partial H}{\partial X} \left(1 - \kappa \left| \frac{\partial H}{\partial X} \right|^{-1} \right)^{1+1/n} \left(1 + \frac{n}{n+1} \kappa \left| \frac{\partial H}{\partial X} \right|^{-1} \right) \right] + $$
$$\lambda (H - Z_1)^{1/n} \left[1 - \frac{1}{\lambda'(H - Z_1)} \right]^{1+1/n} \left[1 + \frac{n}{n+1} \frac{1}{\lambda'(H - Z_1)} \right] = 0, \quad \text{with} \quad \left| \frac{\partial H}{\partial X} \right| > \kappa, \tag{36}$$

where the velocity scale is

$$u^* = \frac{n}{(2n+1)} \left(\frac{\Delta \rho \, g}{\mu_0} \right)^{1/n} \left(\frac{b_0}{2L} \right)^{1+1/n} h_0^{1+1/n}, \tag{37}$$

the time scale is again $t^* = h_0/u^*$, and the coefficient

$$\kappa = \frac{2\tau_p}{\gamma b_0} \frac{L}{h_0} \tag{38}$$

is a non-dimensional number representing the ratio between yield strength and gravity related stress, or the ratio between the Bingham and Ramberg numbers. The boundary and initial conditions are again represented by eq. (21). The coefficients λ and λ' are

$$\lambda = \left(\frac{b_b}{b_0} \right)^{2+1/n} \left(\frac{L}{h_0} \right)^{1+1/n} \left(\frac{h_0}{s} \right)^{1/n}, \tag{39}$$

$$\lambda' = \frac{1}{\kappa_b} \frac{h_0}{s}, \tag{40}$$

where the term κ_b is

$$\kappa_b = \frac{2\tau_p}{\gamma b_b} \frac{L}{h_0} \tag{41}$$

and has the same meaning of κ in eq. (38) but with b_b in place of b_0.

Note that λ defined here for an HB fluid and $r = 0$ is a simplification of that defined in eq. (18) for a power-law fluid, while λ' is the ratio between a vertical hydraulic gradient and

15

κ_b. As such, for $\kappa_b \to 0$ we obtain $\lambda' \to \infty$ and the differential problem reduces to the one developed for a OdW fluid.

In eq. (36), the drainage at the bottom is non-zero if $\lambda'(H - Z_1) > 1$. The presence of yield strength in the fluid produces four possible scenarios, (i) horizontal fracture flow with edge and substrate drainage; (ii) horizontal fracture flow with edge drainage and zero substrate drainage; (iii) no horizontal fracture flow with substrate drainage and zero edge drainage; and (iv) no horizontal flow and zero edge and substrate drainage.

1. Drainage at the substrate only for a HB fluid: the flow during calibration

For estimating the two parameters λ and λ', we proceeded as for an OdW fluid, considering the configuration with drainage only at the substrate according to the schematic in figure 2. While for an OdW fluid it is possible to obtain analytically the evolution (32) of $h(x,t)$, for an HB fluid it is necessary to adopt a numerical procedure. In fact, the vertical flow rate per unit length is equal to

$$q_v = b_0 \left(\frac{b_0}{2}\right)^{1+1/n} \frac{n}{2n+1} \left(\frac{\Delta\rho\,g}{\mu_0}\right)^{1/n} \left(\frac{h - h_0'}{h}\right)^{1/n}$$
$$\times \left(1 - \frac{\kappa h}{h - h_0'}\right)^{1+1/n} \left(1 + \frac{n}{n+1}\frac{\kappa h}{h - h_0'}\right) \quad (42)$$

in the main, rectangular fracture and to

$$q_v = b_b \left(\frac{b_b}{2}\right)^{1+1/n} \frac{n}{2n+1} \left(\frac{\Delta\rho\,g}{\mu_0}\right)^{1/n} \left(\frac{h_0'}{s}\right)^{1/n} \left(1 - \frac{\kappa_b s}{h_0'}\right)^{1+1/n} \left(1 + \frac{n}{n+1}\frac{\kappa_b s}{h_0'}\right), \quad (43)$$

in the bottom crack; in eqs. (42-43), h_0' is the head at $z = 0$.

There is no analytical solution for h_0' in the equation obtained by imposing the invariance of q_v between the main fracture and draining crack. Hence, we cannot express explicitly q_v in the mass conservation equation

$$b_0 \frac{\mathrm{d}h}{\mathrm{d}t} + q_v = 0 \quad (44)$$

written for the bottom crack. Therefore, the solution of the algebraic-differential problem comprising eqs. (42–43) and (44), with the initial condition $h(x,0) = h_0$, is numerical, and can be developed in parametric form in Mathematica[31]: a fitting procedure was adopted between the experimental values $h(t)$ and the model represented by the parametric solution,

estimating s and b_b and calculating λ and λ'. For reference, the estimated values for b_b and s in the three experiments with HB fluids and drainage at the substrate (exp. 13-14-15 in Table I), are $b_b = 0.42, 0.25, 0.37\,\text{mm}$ and $s = 7.9, 7.8, 7.6\,\text{mm}$, respectively. These are quite realistic values if compared to the geometry of the draining fracture adopted in the experimental apparatus.

C.   Numerical integration in space-time

The space-time integration of eq. (19) for Newtonian and power-law fluid, and of eq. (36) for Herschel-Bulkley fluid, with both PDEs subject to eq. (21), is useful to understand the limitations of the self-similar solutions. The integration has been performed with a finite difference method, explicit and predictor-corrector, with some variables estimated in a staggered grid. A test of convergence, performed by comparing the numerical results with the self-similar solution obtained for $n = 1$, shows that a grid with 200 steps guarantees an error less than 0.5%. The time step was selected in order to avoid instabilities, ranging from 10^{-5} to 10^{-8}, with smaller values necessary for more shear-thinning fluids and for larger values of κ in the HB case. Eq. (14) is solved numerically at each step, with the flow rate Q computed at the previous step.

Figure 5 shows the comparison between the self-similar solution for $n = 1$, coincident with the earlier results of Yu *et al.*[15], and the full numerical model at different times. The agreement between the curves is good, with negligible differences.

In order to characterize the behaviour of the solution, a series of numerical simulations were carried out by changing the fluid rheology (Newtonian, OdW shear-thinning with $n = 0.8$, HB with $n = 0.8, 1, \kappa = 1$), the exponent r modulating the aperture variation ($r = 0$ for constant aperture and $r = 1$ for vertical V-shaped cross-section), and $\lambda = 0, 1, 5$.

Figure 6*abc* shows the volume left in the fracture and drained at the substrate and edge, respectively, for Newtonian flow in a constant aperture fracture ($r = 0$), and in a widening aperture ($r = 1$). For the three values $\lambda = 0, 1, 5$ investigated, the increase in permeability along the vertical slows down drainage at early time, when compared to the constant aperture case. At later times, the behaviour for $\lambda = 0$ complies with the theoretical derivation in § II A 2, with the constant aperture fracture emptying faster; for $\lambda > 0$ the trend reverses at late times, when the vertically V-shaped cell empties more rapidly, with an earlier reversal
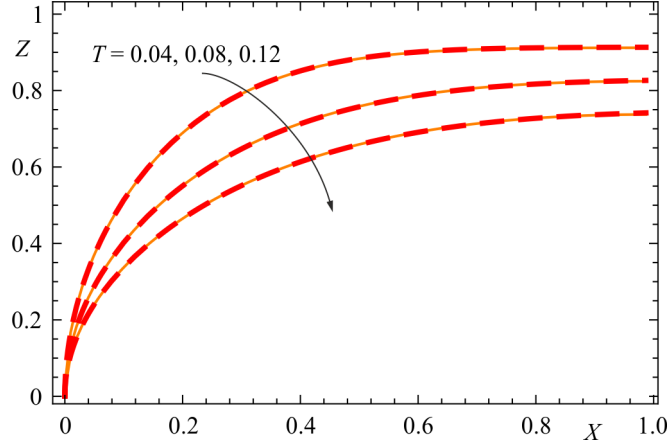
FIG. 5. Comparison between the current profiles computed via numerical integration (dashed red curves) and the self-similar solution (orange bold curves) according to Yu *et al.*[15]. Newtonian fluid with $\lambda = 2$.

the greater is λ.

The drainage at the substrate (null for $\lambda = 0$), on the contrary, increases, while the volume laterally drained reduces. The volume drained at the substrate increases over timebecause the height of the current in the fracture is on average higher, with a relatively high head which boosts the drainage rate. This also applies to shear-thinning fluids (not shown).

Figure 6def compares the results for a Newtonian, a OdW shear-thinning with $n = 0.8$, and a HB fluid ($n = 1, \kappa = 1$) in a constant aperture fracture ($r = 0$). Initially, the fracture empties faster for the shear-thinning than for the Newtonian and HB fluids; the trend is reversed at late times. This result, obtained in the initial phase of drainage and for $\lambda = 0$, is opposite to that theoretically predicted by the self-similar solution in § II A 2, according to which Newtonian behaviour always implies the fastest drainage. The discrepancy between numerical and theoretical results arises from the nature of the self-similar solution, which is an intermediate asymptotics, valid when the initial conditions have been forgotten, whereas the numerical model follows the evolution of the current from the beginning, having continuous memory of the initial conditions. Furthermore, in the numerical model the condition at the draining edge is the critical height and not the null height assumed for the self-similar solution.

The fracture without substrate drainage ($\lambda = 0$) has particularly long emptying times for HB fluids. This follows from the fact that the volume drained at the substrate is greater

for these fluids, while the volume drained at the edge smaller than for both shear-thinning and Newtonian fluids. It should be noted that, in the initial phase of edge drainage, the shear-thinning fluid has higher flow rates than the Newtonian and the HB, as a consequence of the high shear-rates, corresponding to a lower apparent viscosity. In the later stages, the reverse happens, and the volume drained at the edge is slightly higher for the Newtonian fluid.

Results obtained for an HB fluid with $n = 1$ are similar to those obtained with $n = 0.8$ and the same $\kappa = 1$ (not shown). In other possible combinations, for example, the HB fluid has $n < 1$ and higher κ values. In general, the lower the value of n and of κ, the faster the initial emptying of the fracture (not shown). This behaviour is replicated also for the edge drained volumes shown in figure 6f, while it is reversed for the volume drained at the substrate with the same λ, shown in figure 6e.

In order to highlight the combined effects of rheology and fracture geometry on the current behaviour, figure 7 shows a series of profiles calculated for various rheologies and fracture shapes. Figure 7a refers to a Newtonian fluid in a (i) rectangular and (ii) V-shaped fracture, without and with drainage at the substrate. The height of the current in the origin (the draining edge) decreases more slowly for $r = 1$ than for $r = 0$, with greater evidence if the substrate is impermeable ($\lambda = 0$). Conversely, filtration at the bed favours, as expected, a relatively rapid lowering of the profile. The difference between the absence/presence of drainage at the bed is most evident at the terminal stages ($T = 0.01$) of emptying, when the V-shaped cross-section amplifies the level change with an equal volume change. In this regard, we recall that the flow rate over a weir is $\propto h^{3/2}$ (see, e.g., White[32]) and is more sensitive to the height of the current than the flow rate drained at the bed, which is $\propto h$.

Figure 7b compares profiles for a Newtonian and a shear-thinning fluid, in the presence of drainage at the bed and with a V-shaped fracture. In the initial stages ($T < 0.01$), the shear-thinning fluid induces faster drainage than the Newtonian fluid, as a consequence of the lower apparent viscosity when the shear rate is very high. The behaviour reverses, however, for $T > 0.01$, i.e. when the shear-thinning fluid assumes a progressively increasing apparent viscosity. Note that this result is partly influenced by the limitations of the OdW rheological model, which predicts an indefinitely increasing apparent viscosity for shear rates approaching zero. These results also apply to the case of a constant aperture fracture (not shown). We expect these tendencies to be amplified if the fluid is characterized by a
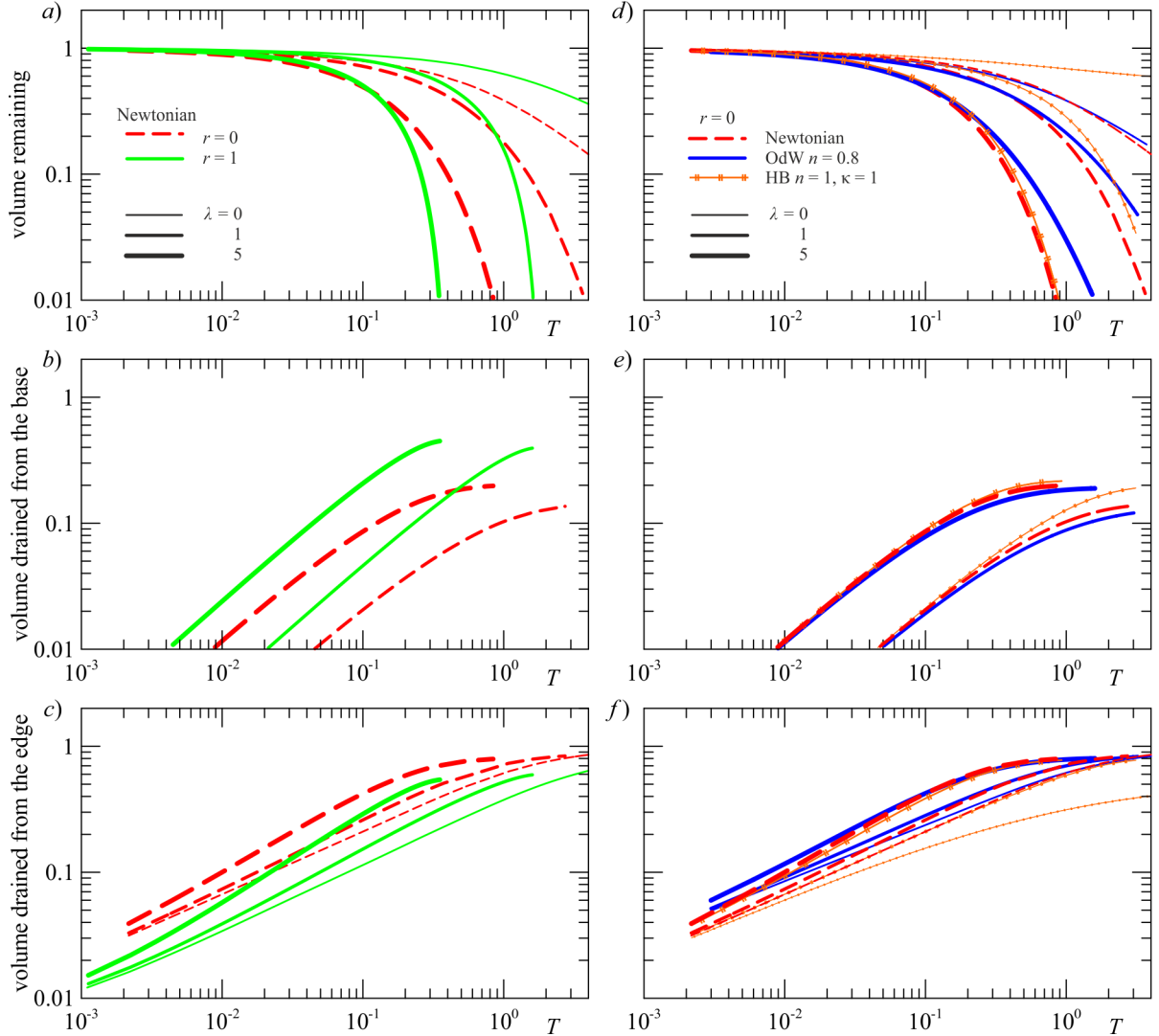
FIG. 6. Volumes remaining, drained at the substrate and at the edge in the fracture. *abc*) Newtonian fluid in a uniform ($r = 0$) and a V-shaped fracture ($r = 1$) for increasing λ; *def*) the effects of fluid rheology in a constant aperture fracture ($r = 0$) for increasing λ.

behaviour index smaller than 0.8.

Figure 7*c* highlights the differences induced by fluid rheology in a constant aperture fracture: the HB and OdW fluids are respectively associated to the slowest and fastest emptying of the fracture, with some important effects of the fluid behaviour index. Note that the yield strength determines a kink in the profile, with a clear separation between the region where the fluid flows and the region where the fluid simply drains from the bed. In the experiments, this behaviour is considerably mitigated: the vertical flow of the HB fluid amplifies the shear rate compared to the theory, so the portion of the domain that

flows since the yield strength is exceeded is larger than its theoretical counterpart. It should be noted that a HB fluid in a fracture without substrate drainage has exceptionally long drainage times, due to the fact that the shear rate is sufficiently high only near the vertical draining end, therefore theoretically most of the domain is a plug, and sooner or later the flux in the whole domain stops. From an experimental point of view, tests performed with an HB fluid without substrate drainage (not shown) indicate that the flow never stops, but emptying times of the fracture are orders of magnitude larger than in the case of substrate drainage.

Finally, it is seen that in the early stages of the evolution of an HB current, a lower n value corresponds to faster drainage; the opposite is true in the later stages. The comparison for different values of κ and n does not qualitatively differ from what has been presented so far, although the regime inversion may occur at different times than those identified in the previous analyses.

III.   EXPERIMENTAL VERIFICATION

The validation of the theoretical model is conducted through the realization of a HS cell to simulate a natural rock fracture. The aperture is uniform along the longitudinal direction, uniform or V-shaped along the vertical, reproducing a porous medium with homogeneous or increasing permeability along the vertical, respectively.

Figure 8 shows the HS cell used during the experiments, 75 cm long and 17 cm high. Boundary conditions allow substrate drainage, which can be started or stopped with a bottom lock-gate; drainage takes place at the bottom through a slot of adjustable width b_b. One end of the HS cell is closed, the other is initially closed with a rubber lock, to be opened during the test to allow lateral (edge) drainage; the drained fluid falls in a container on a scale.

All the experiments are in lock-release configuration, with a constant initial volume. Before each test, the HS cell is filled with fluid through a tube fed by a pump that plugs in the middle of the HS cell, avoiding air bubbles inclusion.

In order to detect the profiles of the current at different times, we used a high-resolution front video camera (Canon Legria HF20 1920 x 1080 pixels) operating at 25 fps. This video camera was referenced through a grid to a lab coordinate system before the beginning of
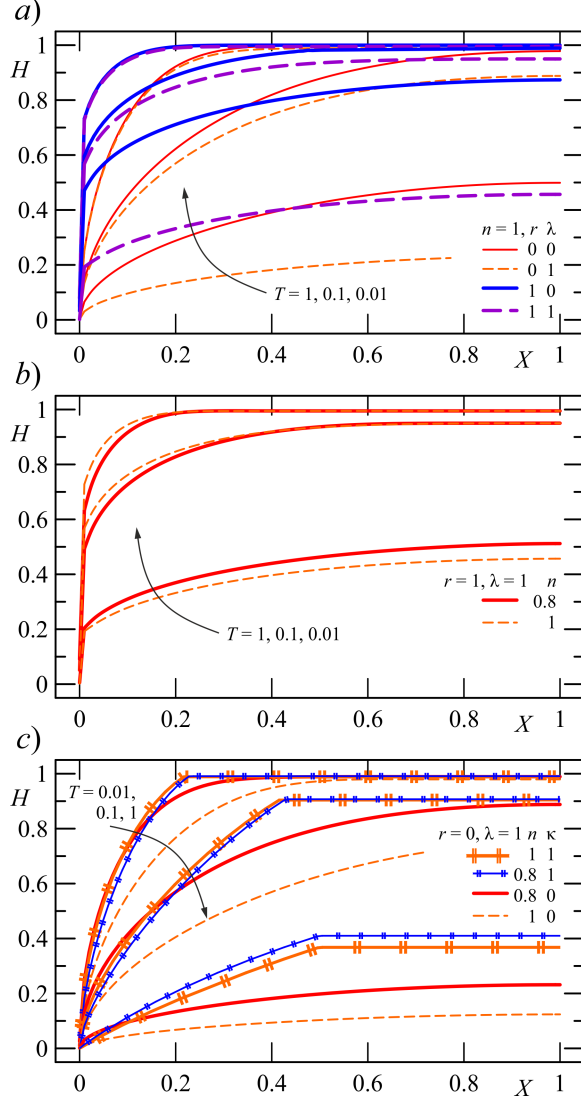
FIG. 7. Profiles of the current at different times. a) Newtonian fluid in a uniform ($r = 0$) and V-shaped fracture ($r = 1$) for $\lambda = 0, 1$; b) Newtonian and shear-thinning OdW fluid in a V-shaped fracture ($r = 1$) for $\lambda = 1$; c) Newtonian, shear-thinning OdW and HB fluids in a constant aperture fracture and $\lambda = 1$. The profiles refer to $T = 0.01, 0.1, 1$.

every test. Then, the fluid leaking from the free edge of the HS cell was piped into a container placed on a scale, with the display recorded by a side camera (iPhone 11 by Apple Inc.) operating at 30 fps, in order to measure the weight of fluid in time.

Each test consisted of two phases. First, calibration allowed the estimation of λ (and λ' for HB fluids in the presence of bottom drainage) value: with the bottom and side gates closed, we filled the HS cell and then, at the start of the calibration phase, quickly opened
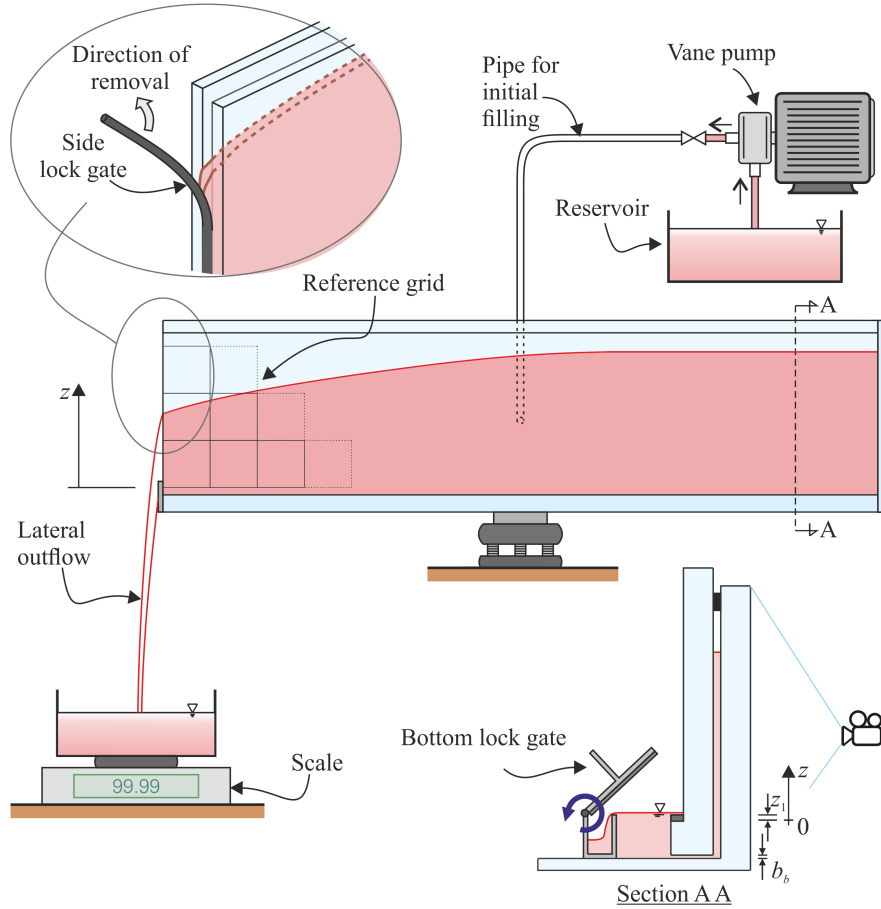
FIG. 8. Schematic of the experimental apparatus used for the experiments.

only the bottom gate to allow the fluid to exit the HS cell by filtering at the bottom. The time variation of the level of the fluid in the HS cell was detected using the front video camera and the λ value was computed by interpolating the theoretical emptying function determined on the basis of mass balance and substrate drainage only, see § II A 3. The second step involved the filtration process from both the side and bottom gates and, for some tests, only from the side one. With both gates closed, we filled the HS cell with fluid

before the start of the experiment and then quickly opened both gates simultaneously. A first set of experiments was conducted using Newtonian fluids, a second one with OdW shear-thinning non-Newtonian fluids and a third one with HB fluids. Newtonian fluids were obtained by mixing glycerol with water, in order to obtain viscosity values that allowed a better observation of the evolution during time of the fluid profiles inside the HS cell. OdW shear-thinning fluids were obtained mixing water, glycerol, and Xanthan Gum (E415) with different concentrations, while HB were obtained mixing water with Carbopol 980 and the correct amount of NaOH to neutralize the solution.

The mass density of the fluids was measured with a Anton Paar DMA 5000 density meter and with a picnometer. The rheologic behaviour of the fluids was analyzed with a Ubbelohde viscometer for Newtonian ones, while for non-Newtonian fluids we used a parallel plate rheometer (Anton Paar Physica MCR 101) conducting rotational tests in order to estimate the consistency index, the fluid behaviour index and, for HB fluids, the yield strength. The shear rate of the rotational tests covered the expected range of the shear rate at the various stages of current evolution in the HS cell during the experiments.

The density of the fluids was measured with an accuracy of $1\,\mathrm{kg\ m^{-3}}$, resulting in $\Delta\rho/\rho \leq 0.1\%$.

The rheological parameters were estimated with a relative uncertainty equal to $\Delta n/n \leq 4\%$ for the fluid behaviour index, to $\Delta\mu_0/\mu_0 \leq 6\%$ for the consistency index, to $\Delta\tau_p/\tau_p \leq 8\%$ for the yield strength. The aperture was known with a relative uncertainty $\Delta b_0/b_0 \leq 5\%$.

The accuracy in measuring the profile of the current is limited by refraction and parallax error, and by tension surface effects, and can be assumed to be $\approx 1\,\mathrm{mm}$, while the time error is half the time interval between two frames, $\approx 1/50 - 1/60\,\mathrm{s}$ for the two cameras. The overall uncertainty in the residual volume is $\leq 7\%$ and the uncertainty in laterally drained volume is associated with the flight time of the fluid from the draining edge to the container on the scale, to the uncertainty in density and mass (weight) measurements, resulting $\leq 2\%$. The uncertainty in the volume filtered at the bottom is $\leq 7.5\%$. The overall uncertainty in the parameter κ is $\Delta\kappa/\kappa \leq 9\%$ and the estimated uncertainty of the bed permeability coefficient is $\Delta\lambda/\lambda \leq 4\%$. For the HB fluids, the second bed permeability coefficient has an uncertainty $\Delta\lambda'/\lambda' \leq 5.5\%$.
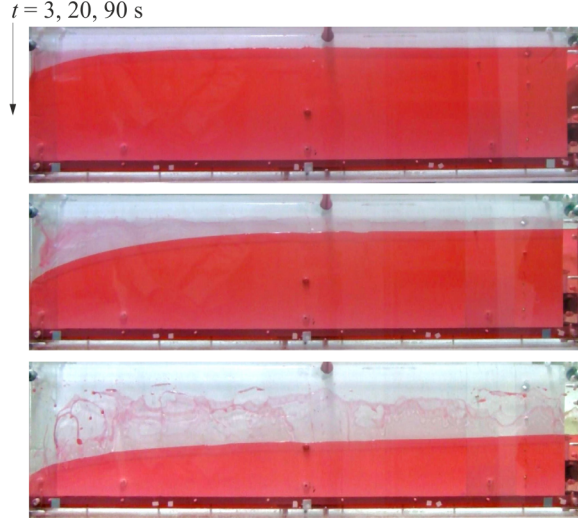
$t = 3, 20, 90$ s

FIG. 9. Snapshots of front video camera acquisitions at $t = 3 - 20 - 90$ s for exp. 9, with both bottom-lock and side-lock gates opened, with a V-shaped geometry of the HS cell and a non-Newtonian OdW shear-thinning fluid. Images are not corrected for distortion.

A. The experiments and their interpretation

Table I lists the experiments and the related parameters. For Newtonian and OdW fluids, the series includes four constant aperture tests, one of which has no filtration at the bed, and two tests with a V-shaped fracture in the vertical direction. For the HB fluid, the tests are only with constant aperture, two of them without filtration at the bed. The absence of tests for HB flow in V-shaped cells was suggested by the tendency of flow blockage in the lower permeability portion of the HS cell, near the permeable bed, which limited the repeatability of the experiments.

Figure 9 shows three snapshots of exp. 9 (numbering refers to table I), and figure 10 shows two examples of rheometric measurements for OdW shear-thinning and HB fluid, respectively.

Figure 11ab shows the time variation of the volume of fluid drained at the bed, at the edge, and remaining in the HS cell for exp. 1. Observing figure 11a, discrepancies between model and experiment are observed mostly in the initial phase, with less fluid exiting the free edge and a slower emptying of the HS cell in the test compared to the theoretical model. Subsequently, the overlap between theory and experiment improves. In general, the discrepancies can be attributed to two phenomena neglected in the theoretical model

25

TABLE I. Parameters for the experiments in the HS cell. ρ is the density of the fluid, n is the fluid behaviour index, μ_0 is the consistency index, τ_p is the yield strength, Θ is the temperature of the fluid during the experiments, b_0 and b_{top} are the aperture at $z = 0$ and at $z = 170\,\text{mm}$, h_0 is the initial level of the fluid in the cell, λ is the dimensionless coefficient for the drainage at the bottom, λ' is the second coefficient for the drainage at the bottom for HB fluids. Letters "u" and "V" stand for "uniform" and "V-shaped", respectively, and E415 is the E-number for Xanthan Gum. The asterisk indicates that the detailed profiles of the currents are shown in the following figures and in the Appendix B.

| Exp.	ρ (kg m^{-3})	n	μ_0 (Pa s^n)	τ_0 (Pa)	Θ (°C)	b_0 (mm)	b_{top} (mm)	h_0 (mm)	λ	λ'	gap	fluid
1*	1241	1.00	0.27		28.1	2.0	2.0	151.5	1.9		u	glyc + H_2O
2	1241	1.00	0.40		28.5	2.0	2.0	157.7	6.4		u	
3	1246	1.00	0.44		25.0	3.0	3.0	156.0	22.5		u	
4	1245	1.00	0.45		27.5	0.5	2.8	164.7	5.0		V	
5*	1249	1.00	0.59		25.3	1.0	3.5	160.0	9.0		V	
6	1255	1.00	0.29		23.5	2.5	2.5	160.6	0.0		u	
7	1075	0.35	1.31		29.0	2.0	2.0	139.1	241.0		u	glyc +H_2O + E415
8	1185	0.43	1.18		25.8	2.0	2.0	137.0	25.0		u	
9*	1216	0.56	0.99		25.3	3.0	3.0	154.6	4.0		u	
10*	1218	0.56	1.07		23.8	0.5	2.9	156.0	22.5		V	
11	1215	0.56	0.97		24.3	1.0	3.5	154.6	35.0		V	
12	1066	0.39	1.15		23.3	2.0	2.0	150.2	0.0		u	
13*	1000	0.52	2.20	0.24	21.8	3.0	3.0	150.5	14.1	32.5	u	H_2O + Carbopol
14	1000	0.70	0.55	0.60	20.4	2.0	2.0	153.3	2.7	7.8	u	
15	1000	0.80	0.85	0.30	20.7	2.0	2.0	153.0	6.5	23.9	u	
16	1000	0.60	0.40	0.35	19.8	2.0	2.0	144.4	0.0		u	
17	1000	0.72	0.70	0.30	22.4	2.0	2.0	146.2	0.0		u	
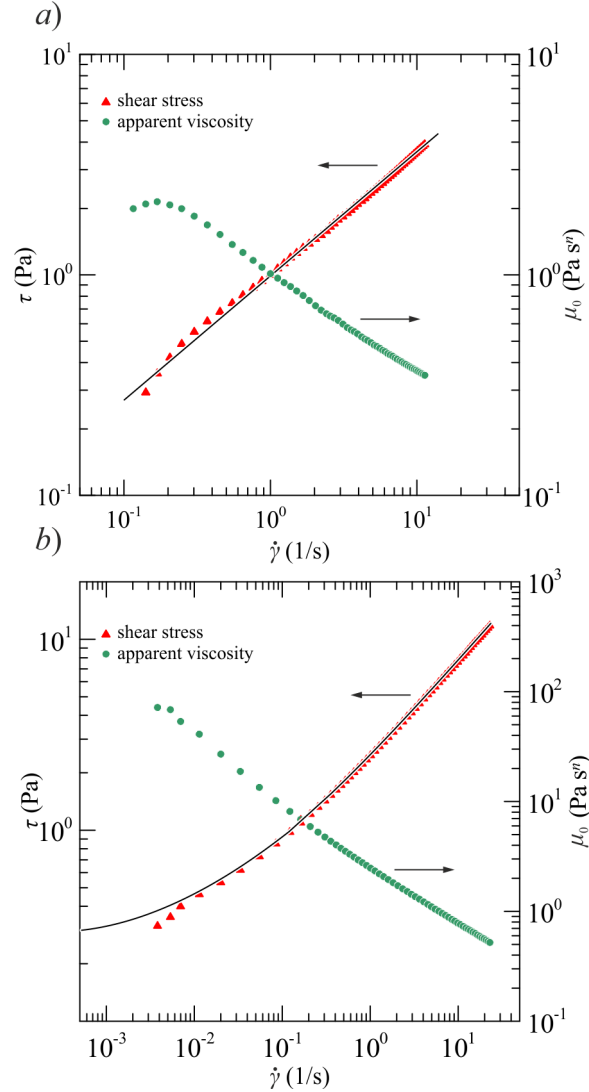
FIG. 10. Rheometry of the fluids. a) OdW shear-thinning fluid, and b) HB fluid. Triangles are the measured shear-stress vs shear-rate, circles are the computed apparent viscosity vs shear-rate, with symbols decimated for better visualization. Bold lines are the interpolating curves.

adopted: i) the effects of surface tension and ii) the strong curvature of trajectories of fluid particles. The surface tension between the walls of the HS cell and the fluid produces additional resistance, while that between fluid and air at the draining edge favours a localized flow increase (a similar effect occurs in thin-walled Bazin-type weirs. Moreover, in the initial stages of the phenomenon (for example at 10-20 s), there is a strong curvature of the trajectories of fluid particles; this increases the head gradient and thus favours outflow. As to the configuration of exp. 1, it is evident that the tension surface at the air-wall-liquid interface dominates the process. This aspect is even more evident in figure 11a, where the

27
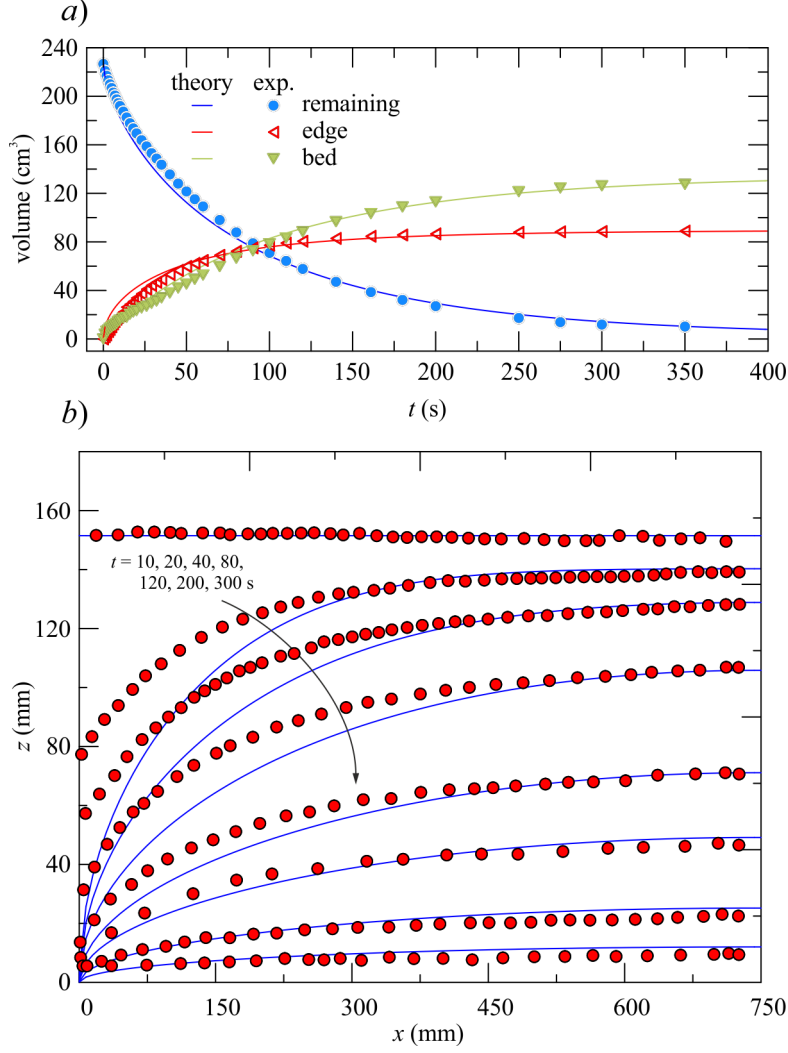
FIG. 11. Newtonian fluid with coupled drainage in a constant aperture fracture. *a*) Time variation of the volume remaining in the fracture and drained from the edge and at the bed; *b*) current profiles at different times. Symbols are the experiments, curves are the numerical results. Exp. 1 in table I, $\lambda = 1.9$.

theoretical profiles at initial times largely underestimate the experimental values near the free draining edge, but then fit the experiments quite well at later stages, when the strong curvature of the free surface and trajectories disappears.

Similar results are shown, for different fluids and geometry of the HS cell, in Appendix B.

The experimental and theoretical residual volumes in the HS cell as a function of time are shown in figure 12 for all tests. Several parameters are involved in determining the volume evolution in the HS cell, and the interplay between them makes it difficult to identify a

clear trend. Some tests (expts. 6-12-16-17) were performed without filtration at the bottom ($\lambda = 0$) and show a slower reduction in residual volume than the other tests in which drainage was also at the bottom. We can observe how the theoretical variation in residual volume predicted by the self-similar solution, applicable in exp. 6 and exp. 12, is adequately reproduced for very long times. The repeatability of the two tests performed with HB fluid, exp. 16 and 17, is clearly seen from figure 12c. The effect of very intense drainage at the bottom, as is the case for exp. 7 in figure 12b, is also evident. In the tests with a V-shaped HS cell (exp. 4 and 5 in figure 12a and exp. 10 and 11 in figure 12b), the sensitivity to the value of the parameter λ is lower.

The volume of drained fluid, from the edge and at the substrate, is shown in figure 13. It is seen that theoretical predictions of drained volumes are a good match of experimental results, except at very early times, when the self-similar solution is not yet applicable. Results for all fluids and both drained volumes, edge and substrate, show a clear dependency on fluid parameters, the λ parameter, and the fracture shape (uniform or V-shaped). As expected, larger values of λ (see exp. 7 and exp. 13) imply a higher substrate drained volume, while a uniform aperture entails a larger volume drained at the substrate with respect to the V-shaped fracture, see the comparison between exp. 8 and exp. 10 with similar values of λ. At large times, the sum of (dimensionless) drained volumes tends to one as the fracture empties.

Figure 14 shows the temporal evolution of the theoretical critical height at the drainage edge. There is an initial phase with a height decay according to a power function, followed by a phase of more rapid reduction. The initial slope of the curves is a function of the rheological characteristics of the fluid, but also of the value of λ. Indeed, in experiments performed with $\lambda = 0$, the decay is noticeably slower, while very high values of λ induce a fast decay. The effect of λ on the height decay at the edge is particularly high for OdW shear-thinning fluids; for these the modulation of the apparent viscosity, which increases as the profile curvature decreases, also plays a role. For HB fluids, which share a shear-thinning behaviour when flowing, this effect is masked by yield strength, which prevents too rapid a reduction. For HB fluids, the tests indicate that even after a long time the critical height is not negligible, though small. For experiments with comparable values of λ, in the early stage $H_c \propto T^{-0.4}$ for Newtonian fluids (exp. 3), $H_c \propto T^{-0.65}$ for shear-thinning fluids (exp. 10), and $H_c \propto T^{-0.5}$ for HB fluids (exp. 13).
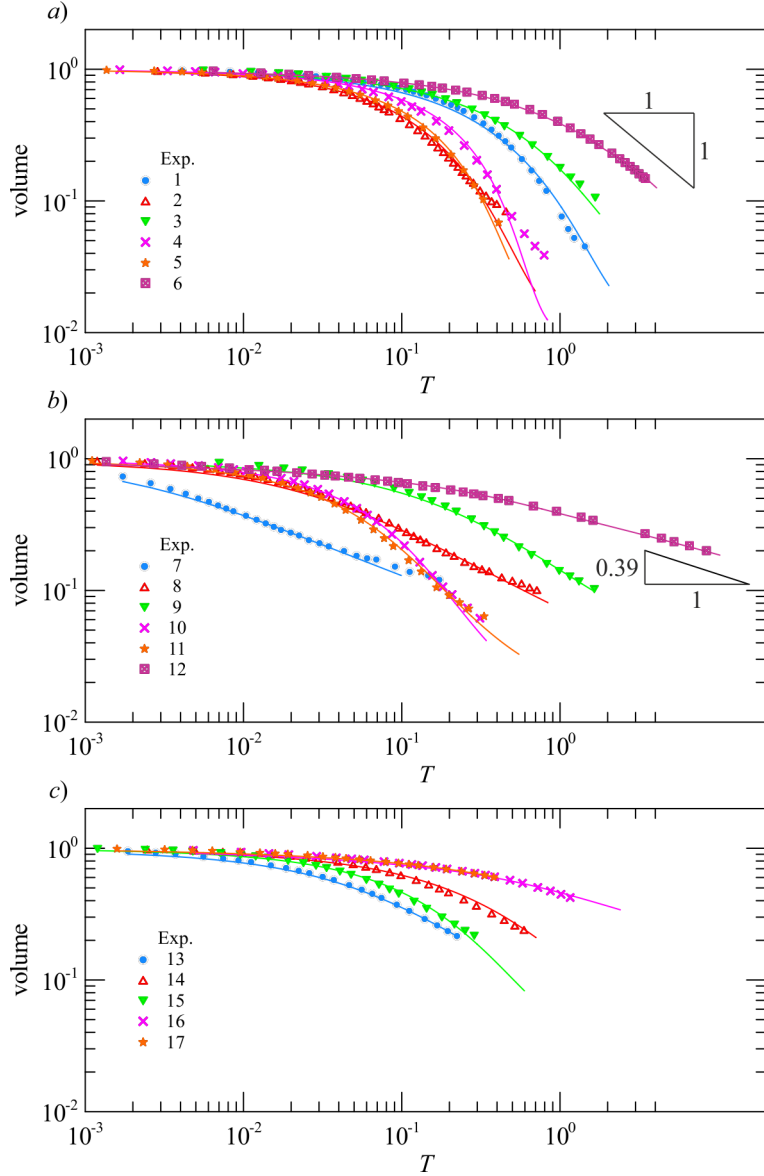
FIG. 12. Residual fluid volume in the HS cell as a function of time. a) Newtonian fluids; b) OdW shear-thinning fluids, and c) HB fluids. For a constant aperture fracture without bottom drainage, the residual volume theoretically decays as T^{-1} for Newtonian (exp. 6), and as T^{-n} for power-law fluid (exp. 12).
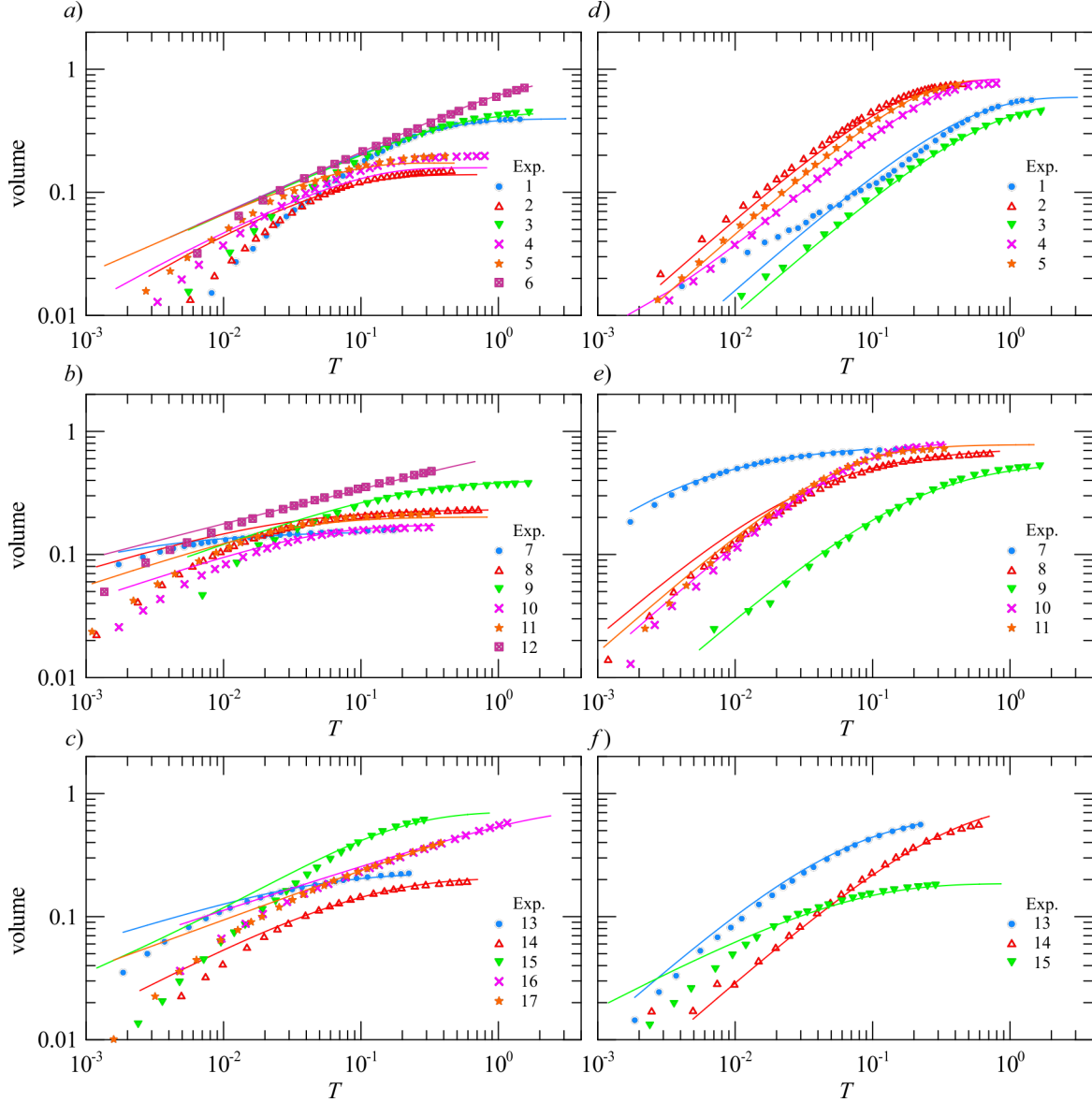
FIG. 13. Time variation of outgoing fluid volume, at the edge (left column) and at the substrate (right column). *a-d*) Newtonian fluids; *b-e*) OdW shear-thinning fluids, and *c-f*) HB fluids.
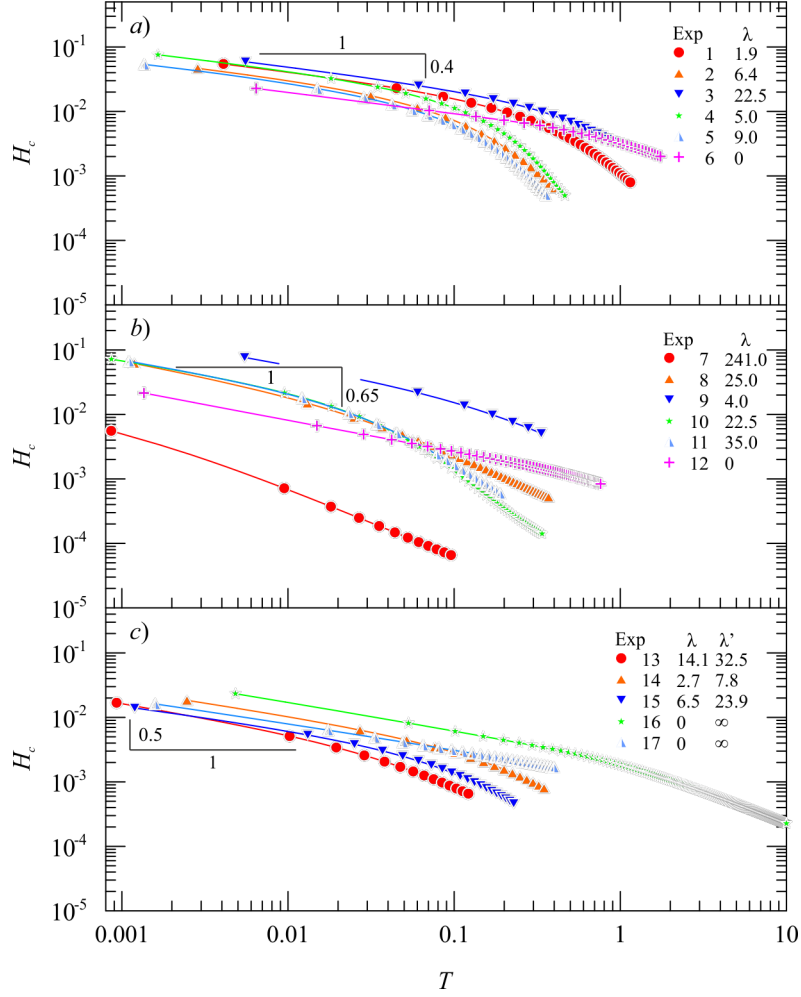
FIG. 14. Dimensionless theoretical height of current at the draining edge H_c, as a function of time T. a) Newtonian fluids; b) OdW shear-thinning fluids, and c) HB fluids. Experimental values of the current height at the edge are unavailable due to distortions induced by surface tension.

IV. CONCLUSION

In this paper, we have theoretically analyzed, and experimentally verified, the evolution of a viscous current rheologically described by the Newtonian, Ostwald-deWaele, and Herschel-Bulkley models and subject to coupled drainage from a lateral edge and the substrate in a fracture schematized by a Hele-Shaw cell. The cell takes both a constant and linearly variable, V- shaped aperture, also representing the case of a porous medium with increasing permeability and porosity. The initial condition is of completely filled cell, constant volume and no inflow rate later on. The problem, for the case of lateral drainage only and a Ostwald-deWaele fluid, admits a self-similar solution, derived here as an extension of the Newtonian fluid solution in[14]. It also admits a self-similar solution for a Newtonian fluid in a constant aperture fracture with coupled drainage[15]. In all other configurations, the solution is obtained numerically.

In the numerical solution, the depth at the vertical draining edge is taken to be the critical height, which corresponds to the minimum specific energy for an assigned discharge. In the self-similar solution, the depth is taken to be zero as the solution is an intermediate asymptotic, valid at late time.

Comparison with experimental results, both for integral variables such as the residual volume in the cell and the volume drained at the edge and at the bed, and for current profiles as a function of time, confirms the validity of the model and the reliability of the numerical computations. Discrepancies between experiments and theory are mainly found for the initial phases of the fracture emptying, when the strong spatial gradients of the height of the current invalidate the assumption of zero vertical velocity, while the surface tension contributes to deviations from the dynamics embedded in the model.

The emptying time of the fracture is dependent on the rheology, as well as the vertical variability of the aperture, and is generally lower for Newtonian than for the other fluids investigated. However, if one changes the boundary condition at the edge, imposing the critical height instead of a null height, the initial stages may result in the shear-thinning fluid draining faster than the Newtonian. In the case of no drainage at the substrate and for a constant aperture fracture, the residual volume decays according to $\sim T^{-1}$ for Newtonian (exp. 6), and according to $\sim T^{-n}$ for power-law fluid (exp. 12), as predicted by the theoretical dependence $\sim T^{-n/[r(n+1)+1]}$ for a power-law fluid in a V-shaped fracture.

Of particular interest is the extension to HB fluids, with an emptying dynamics which is controlled by clogging when the maximum tangential stresses do not exceed the yield strength. Four scenarios arise, depending whether lateral and bottom drainage are both present, or one of them is null due to clogging, or both are null, again due to clogging. The experiments conducted for HB fluids refer only to a fracture of constant width and with filtration at the bottom generated by a crack. It will be important to extend the analysis to the case where drainage to the bottom is due to a porous medium, for which the transition between flow and no-flow situations is not as sharp as it is for a fracture, but grows progressively as documented in the experiments of Chevalier *et al.*[33].

The analysis conducted here is of interest in the study of CO_2 sequestration, as some CO_2-rich solutions used for carbon dioxide capture display non-Newtonian rheology[26], and the substrate leakage term and the fracture emptying times are heavily affected by the value of the rheological index. Applications are not limited to CO_2 sequestration, but involve process fluids adopted in aquifer remediation and oil recovery, which frequently have markedly non-Newtonian behaviour[25,34].

Appendix A: The calibration of the λ value for OdW fluids

The calibration of the λ value was performed considering flow in the absence of edge drainage, with a constant aperture fracture ($r = 0$) initially full and gradually emptying with a discharge that can be calculated on the basis of the geometry and the rheological
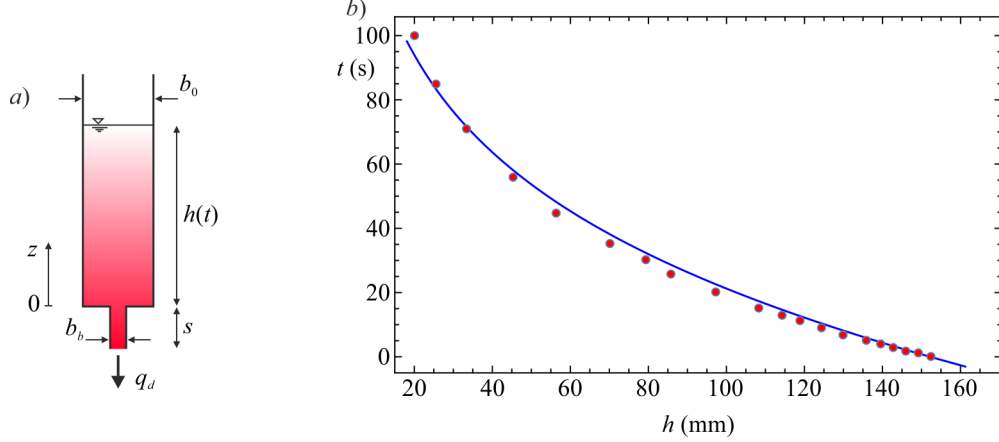
FIG. A.1. Calibration of the λ parameter. *a*) Schematic of the flow geometry during calibration; *b*) Curve-fitting of the experimental data with eq. (32); configuration of exp. 2, Newtonian fluid in a constant aperture fracture, case with substrate drainage only. The calibrated value is $\lambda = 6.4$.

characteristics of the fluid. Based on the schematic in figure A.1a representing the cross-section of the experimental apparatus, the flow rate per unit width in the cell is equal to

$$q_v = b_0 \left(\frac{b_0}{2}\right)^{(n+1)/n} \frac{n}{2n+1} \left(\frac{\Delta\rho\,g}{\mu_0}\right)^{1/n} \left(\frac{h-h_0'}{h}\right)^{1/n}, \tag{A1}$$

where h_0' is the head at $z = 0$. The same flow rate per unit width applies to the smaller meander, for which we can write

$$q_v = b_b \left(\frac{b_b}{2}\right)^{(n+1)/n} \frac{n}{2n+1} \left(\frac{\Delta\rho\,g}{\mu_0}\right)^{1/n} \left(\frac{h_0'}{s}\right)^{1/n}, \tag{A2}$$

having neglected the concentrated head losses at the contraction at $z = 0$. Deriving h_0' from eq. (A2) and substituting in eq. (A1) results in

$$q_v \equiv q_d = \frac{b_0 \left(\frac{b_0}{2}\right)^{(n+1)/n} \frac{n}{2n+1} \left(\frac{\Delta\rho\,g}{\mu_0}\right)^{1/n}}{\left[1 + \left(\frac{b_0}{b_b}\right)^{2n+1} \frac{s}{h}\right]^{1/n}}, \tag{A3}$$

representing the drainage rate during the emptying process. Having defined $V = b_0 h$ as the fracture volume per unit longitudinal fracture length, mass conservation in the HS cell requires that

$$\frac{\mathrm{d}V}{\mathrm{d}t} = -q_d \rightarrow \frac{\mathrm{d}h}{\mathrm{d}t} = -\frac{\left(\frac{b_0}{2}\right)^{(n+1)/n} \frac{n}{2n+1} \left(\frac{\Delta\rho\,g}{\mu_0}\right)^{1/n}}{\left[1 + \left(\frac{b_0}{b_b}\right)^{2n+1} \frac{s}{h}\right]^{1/n}}, \tag{A4}$$
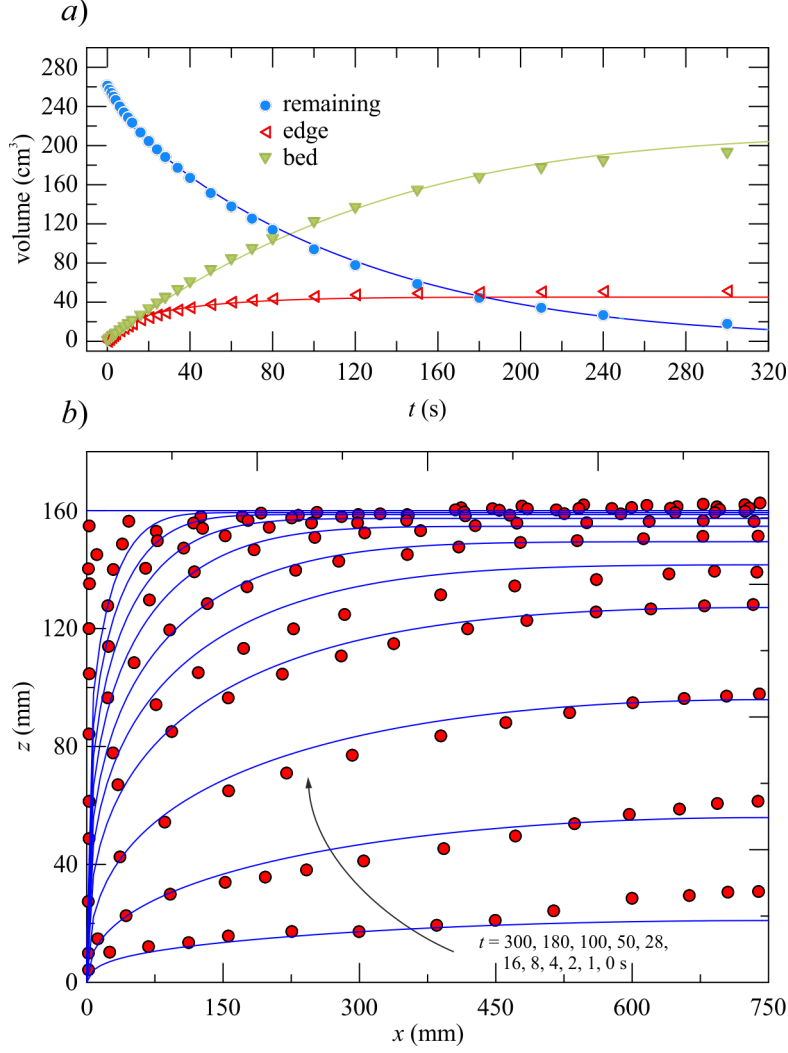
35

FIG. B.2. Newtonian fluid with coupled drainage in a V-shaped fracture, exp. 5 in table I, $\lambda = 9.0$. For caption, see figure 11.

resulting in eq. (31). Figure A.1b shows the interpolation of experimental values for exp. 2.

Appendix B: The details of some experiments

Figure B.2ab shows the results of the comparison between theory and experiments for exp. 5, with a Newtonian fluid in a vertically V-shaped HS cell. Again, the comparison is fairly good. Note the effect of the V-shaped fracture on the current profile: near the draining edge the curvature of the free surface is greater than for a constant aperture fracture, as a result of the higher permeability at a higher elevation from the bottom.

Figure B.3ab refers to a OdW shear-thinning fluid in a constant aperture fracture. It is
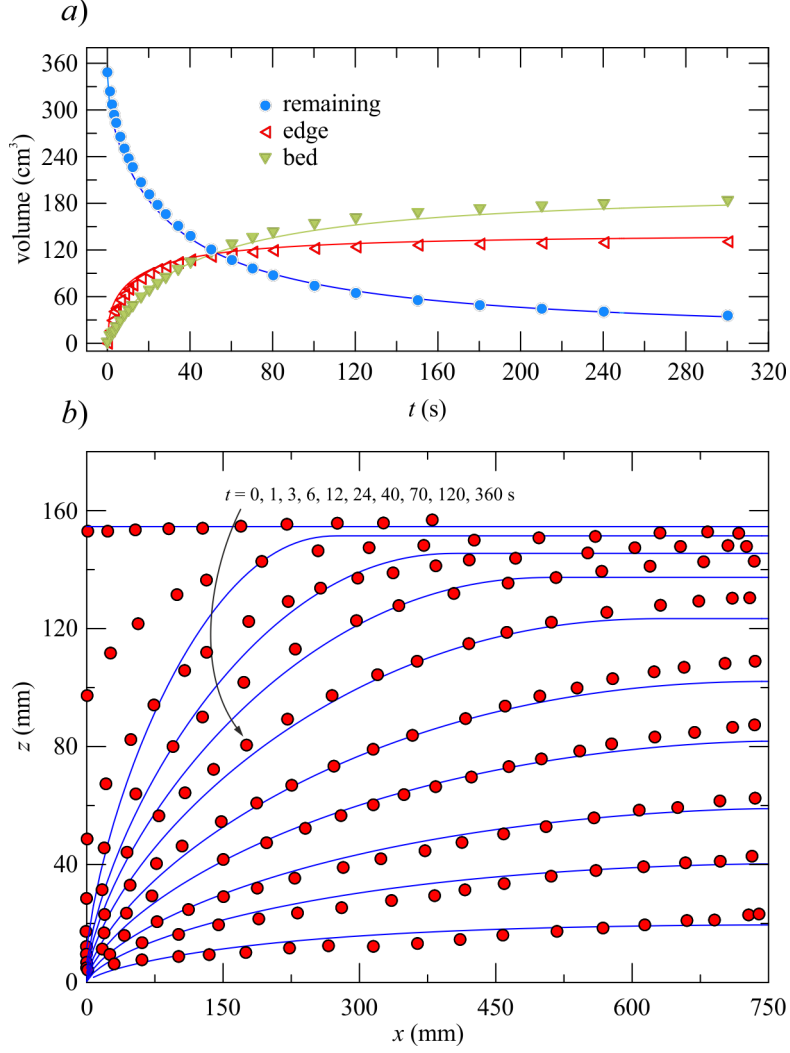
FIG. B.3. Ostwald-deWaele shear-thinning fluid with coupled drainage in a constant aperture fracture, exp. 9 in table I, $\lambda = 4.0$. For caption, see figure 11.

evident that the lower apparent viscosity in the initial phase, when the shear-rate is particularly high, facilitates drainage from the draining edge, with the HS cell emptying faster than for a Newtonian fluid. As in the other experiments, the theoretical profile at early times underestimates the height of the current near the origin, although the difference quickly disappears as time increases, with a good overlap between theory and experiments. A similar behaviour is observed if the HS cell is V-shaped, see figure B.4, in which, as was already the case for the Newtonian fluid, the curvature of the profile near the origin is enhanced by the permeability decreasing towards the bottom. The theoretical profile systematically underestimates the experimental data near the closed end and, as always, near the origin at

early time.

The profiles and volumes for an HB fluid are shown in figure B.5. The profiles are characterized by a kink separating the region of the domain where the shear-stress is sufficient to overcome the yield strength, from the region where, if no drainage were present at the bottom, the fluid would remain at rest. It should be noted that the experiments do not exhibit such a kink, as: i) the resolution of the experimental data is not high enough to capture the localized variation in slope, and ii) the actual flow field, especially in the presence of substrate flow, is more complex than that schematized by the model. In practice, if instead of the shallow water scheme, which neglects the curvature of the trajectories and, therefore, the vertical velocity, we were to use a scheme capable of considering this curvature, we would estimate a higher mobility of the fluid, closer to that experimentally inferred.
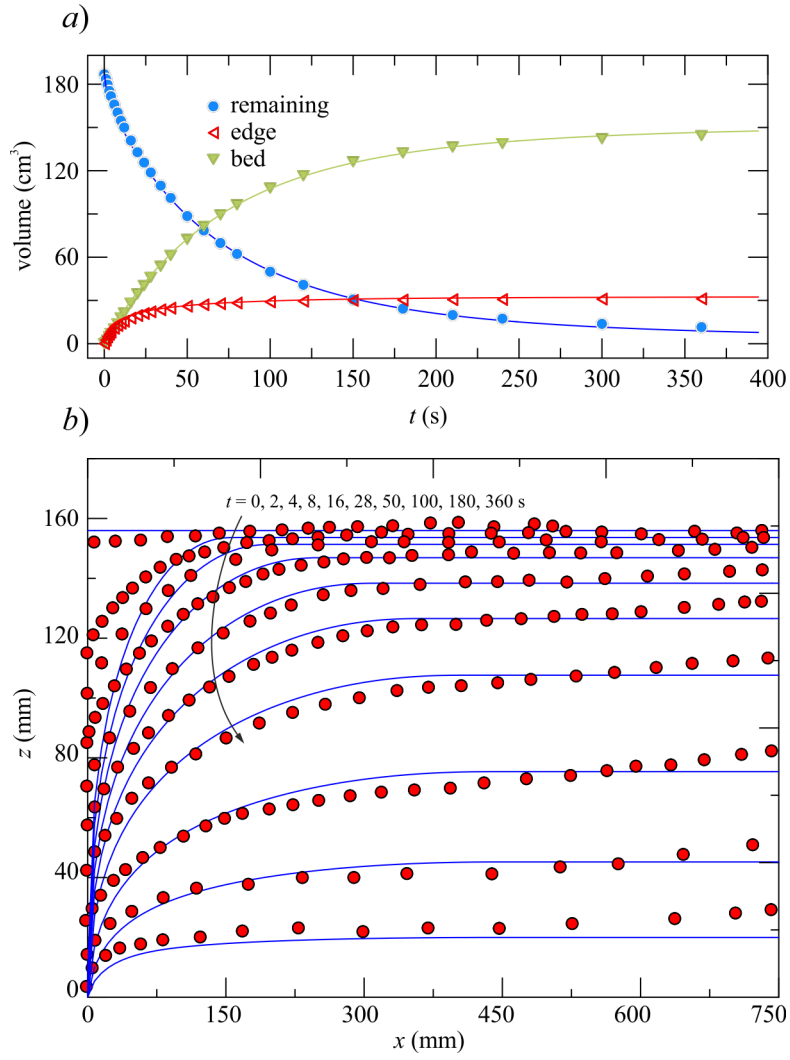
FIG. B.4. Ostwald-deWaele shear-thinning fluid with coupled drainage in a V-shaped fracture, exp. 10 in table I, $\lambda = 22.5$. For caption, see figure 11.
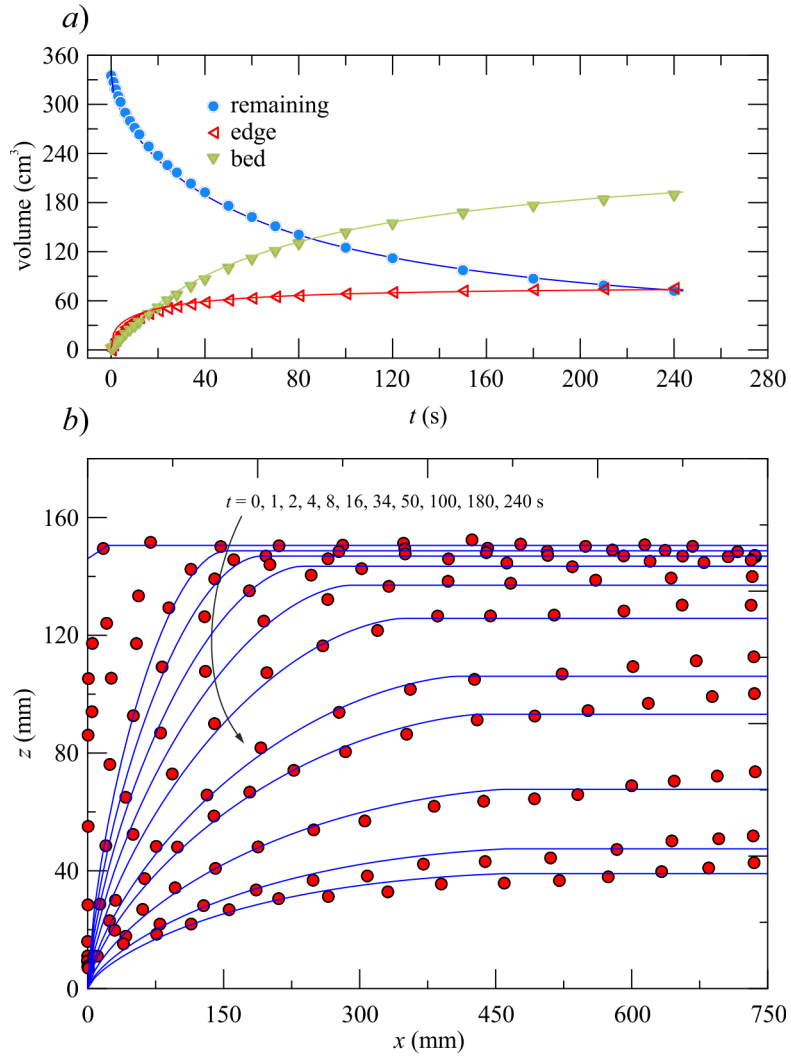
FIG. B.5. HB fluid with coupled drainage in a constant aperture fracture, exp. 13 in table I, $\lambda = 14.1$. $\lambda' = 32.5$. For caption, see figure 11.

REFERENCES

[1] J. E. Simpson, *Gravity currents in the environment and the laboratory* (Cambridge University Press, 1997).

[2] H. E. Huppert, "The intrusion of fluid mechanics into geology," Journal of Fluid Mechanics **173**, 557–598 (1986).

[3] M. Ungarish, *Gravity Currents and Intrusions: Analysis and Prediction* (World Scientific, 2020).

[4] S. Lyle, H. Huppert, M. Hallworth, M. Bickle, and A. Chadwick, "Axisymmetric gravity currents in a porous medium," Journal of Fluid Mechanics **543**, 293–302 (2005).

[5] D. Vella and H. E. Huppert, "Gravity currents in a porous medium at an inclined plane," Journal of Fluid Mechanics **555**, 353–362 (2006).

[6] D. Vella, J. A. Neufeld, H. E. Huppert, and J. R. Lister, "Leakage from gravity currents in a porous medium. part 2. a line sink," Journal of Fluid Mechanics **666**, 414–427 (2011).

[7] T. Goda and K. Sato, "Gravity currents of carbon dioxide with residual gas trapping in a two-layered porous medium," Journal of Fluid Mechanics **673**, 60–79 (2011).

[8] S. Longo, V. Di Federico, L. Chiapponi, and R. Archetti, "Experimental verification of power-law non-Newtonian axisymmetric porous gravity currents," Journal of Fluid Mechanics **731, R2**, 1–12 (2013).

[9] S. Longo, V. Di Federico, and L. Chiapponi, "A dipole solution for power-law gravity currents in porous formations," Journal of Fluid Mechanics **778**, 534–551 (2015).

[10] V. Ciriello, V. Di Federico, R. Archetti, and S. Longo, "Effect of variable permeability on the propagation of thin gravity currents in porous media," International Journal of Non-Linear Mechanics **57**, 168–175 (2013).

[11] V. Di Federico, S. Longo, L. Chiapponi, R. Archetti, and V. Ciriello, "Radial gravity currents in vertically graded porous media: theory and experiments for Newtonian and power-law fluids," Advances in Water Resources **70**, 65–76 (2014).

[12] J. M. Acton, H. E. Huppert, and M. G. Worster, "Two-dimensional viscous gravity currents flowing over a deep porous medium," Journal of Fluid Mechanics **440**, 359–380 (2001).

[13] D. Pritchard, "Gravity currents over fractured substrates in a porous medium," Journal of Fluid Mechanics **584**, 415–431 (2007).

[14] Z. Zheng, B. Soh, H. E. Huppert, and H. A. Stone, "Fluid drainage from the edge of a

porous reservoir," Journal of Fluid Mechanics **718**, 558–568 (2013).

[15]Y. E. Yu, Z. Zheng, and H. A. Stone, "Flow of a gravity current in a porous medium accounting for drainage from a permeable substrate and an edge," Physical Review Fluids **2**, 074101 (2017).

[16]S. Longo, V. Di Federico, and L. Chiapponi, "Propagation of viscous gravity currents inside confining boundaries: the effects of fluid rheology and channel geometry," Proceedings of the Royal Society of London A: Mathematical, Physical and Engineering Sciences **471** (2015), 10.1098/rspa.2015.0070.

[17]I. Lauriola, G. Felisa, D. Petrolo, V. Di Federico, and S. Longo, "Porous gravity currents: Axisymmetric propagation in horizontally graded medium and a review of similarity solutions," Advances in Water Resources **115**, 136–150 (2018).

[18]V. Di Federico, S. Longo, S. E. King, L. Chiapponi, D. Petrolo, and V. Ciriello, "Gravity-driven flow of Herschel–Bulkley fluid in a fracture and in a 2D porous medium," Journal of Fluid Mechanics **821**, 59–84 (2017).

[19]F. Zeighami, A. Lenci, and V. Di Federico, "Drainage of power-law fluids from fractured or porous finite domains," Journal of Non-Newtonian Fluid Mechanics **305**, 104832 (2022).

[20]V. Ciriello, S. Longo, L. Chiapponi, and V. Di Federico, "Porous gravity currents: a survey to determine the joint influence of fluid rheology and variations of medium properties," Advances in Water Resources **92**, 105 – 115 (2016).

[21]S. Longo, L. Chiapponi, D. Petrolo, A. Lenci, and V. Di Federico, "Converging gravity currents of power-law fluid," Journal of Fluid Mechanics **918**, A5 (2021).

[22]Z. Zheng and H. A. Stone, "The influence of boundaries on gravity currents and thin films: drainage, confinement, convergence, and deformation effects," Annual Review of Fluid Mechanics **54**, 27–56 (2022).

[23]M. E. Thompson and S. R. Brown, "The effect of anisotropic surface roughness on flow and transport in fractures," Journal of Geophysical Research: Solid Earth **96**, 21923–21932 (1991).

[24]D. T. Snow, "Anisotropie permeability of fractured media," Water Resources Research **5**, 1273–1289 (1969).

[25]K. R. Chaturvedi, R. Narukulla, J. Trivedi, and T. Sharma, "Effect of single-step silica nanoparticle on rheological characterization of surfactant based CO_2 foam for effective carbon utilization in subsurface applications," Journal of Molecular Liquids **341**, 116905

(2021).

26M. Zalewski, T. Krawczyk, A. Siewniak, and A. Sobolewski, "Carbon dioxide capture using water-imidazolium ionic liquids-amines ternary systems," International Journal of Greenhouse Gas Control **105**, 103210 (2021).

27D. Pritchard and A. J. Hogg, "Draining viscous gravity currents in a vertical fracture," Journal of Fluid Mechanics **459**, 207–216 (2002).

28D. Pritchard, A. W. Woods, and A. J. Hogg, "On the slow draining of a gravity current moving through a layered permeable medium," Journal of Fluid Mechanics **444**, 23–47 (2001).

29V. T. Chow, *Open-channel hydraulics* (McGraw-Hill, 1959).

30S. Longo, *Principles and Applications of Dimensional Analysis and Similarity* (Springer, 2022).

31Wolfram Research, Inc., "Mathematica, Version 11.1," (2017), champaign, IL, 2017.

32F. White, ed., *Fluid Mechanics* (Mc-Graw-Hill, 1979).

33T. Chevalier, C. Chevalier, X. Clain, J. C. Dupla, J. Canou, S. Rodts, and P. Coussot, "Darcy's law for yield stress fluid flowing through a porous medium," Journal of Non-Newtonian Fluid Mechanics **195**, 57–66 (2013).

34M. Theodoropoulou, V. Karoutsos, and C. Tsakiroglou, "Investigation of the contamination of fractured formations by non-newtonian oil pollutants," Environmental Forensics **2**, 321–334 (2001).